JOURNAL OF APPLIED GEOSPATIAL INFORMATION

Vol 8 No 1 2024

http://jurnal.polibatam.ac.id/index.php/JAGI
ISSN Online: 2579-3608

Ionic Geospatialization and Hydrochemical Characterization of Water Resources around Selected Petroleum Producing Areas in South-Southern Nigeria

Nurudeen Onomhoale Ahmed [1, *], Mohammed Bashir Suleiman [2], Finjite Dorathy Olali [3], Mojisola Mary Ogunkoya [4], Fayose Olalekan Oluwatobi [5], Deborah Ifesinachi Elom-Nwuzor [6]

[1] *Institute of Natural Resources, Environment and Sustainable Development (INRES), University of Port Harcourt, Nigeria*
[2] *Department of Geology, Faculty of Physical Sciences, University of Maiduguri, Nigeria*
[3] *Department of Geology, Faculty of Natural Sciences, University of Port Harcourt, Nigeria*
[4] *Department of Environmental Management, School of Health and Life Sciences, Teesside University, United Kingdom*
[5] *Department of Geology, Faculty of Physical Sciences, Federal University Oye Ekiti, Nigeria*
[6] *Department of Geology, Faculty of Physical Sciences, University of Benin, Nigeria*
* *Corresponding Author: nurudeenonomhoale@gmail.com*

Received: April, 01 2024
Accepted: June 11, 2024
Published: June 11, 2024

Abstract

Water resources play a crucial role in sustaining life and various socio-economic activities, especially in regions like South-Southern Nigeria, where petroleum production activities are prevalent. This study focuses on understanding the hydrochemical characteristics and geospatial distribution of major ions in water around selected petroleum-producing areas, notably within the Obigbo Local Government Area (L.G.A) of Rivers State. A total of 41 water samples, comprising 34 rain and 7 surface waters, were collected, and analyzed employing hydrochemical modeling techniques, including the Piper Trilinear plot, Durov, and Schoeller diagram, to characterize the ionic composition of surface water and rainwater. The analysis revealed a relatively uniform pattern of major ions, including Ca, Mg, Na, K, HCO3, Cl, SO4, and NO3, across the study area, with higher concentrations observed along the river channel, in the Northern regions. Rainwater samples exhibited lower concentrations, with discernible variations, especially in areas adjacent to petroleum activities. The dominance of Ca + Mg as cations and Cl as anions was consistent in both river water and rainwater samples. Durov diagram depicted a simple dissolution or mixing line in river water, while rainwater samples exhibited a notable presence of calcium and sulphate. The Schoeller diagram indicated a calcium chloride water type, with rainwater showing heightened calcium and sulphate concentrations. Geospatial analysis highlighted consistent ion concentration levels throughout the study area, suggesting environmental stability. Despite concerns about increased sulfate near petroleum facilities, all measured ion concentrations in both river and rainwater samples adhered to WHO standards, indicating satisfactory water quality.

Keywords: Ionic Geospatialization, Hydrochemical Characterization, Major Ions Analysis, Water Resource Assessment, Rivers State, South-Southern Nigeria

1. Introduction

In the ever-evolving landscape of hydrogeology and environmental science, the significance of water to mankind remains unequivocal. Water, indispensable for households, agriculture, and industries, forms the bedrock of human existence (Ochelebe and Kudamnya, 2022; Idris et al., 2021; Tiwari et al., 2017; Roșca et al., 2020). With about three-quarters of the Earth's surface covered by water, its importance cannot be overstated. However, a mere three percent of the Earth's water resources

are freshwater, with the majority locked in saline oceans and seas (Cidu et al., 2011).

Within the study area, comprising selected petroleum producing regions in South-Southern Nigeria, water resources are predominantly sourced from precipitation, surface, and groundwater reservoirs (Ahmed et al., 2024a). Surface water sources, including rivers and streams, coexist with groundwater within subterranean aquifers, both shallow and deep (Edet, 2018). Gas flaring, a prevalent practice the South-Southern of Niger Delta region of Nigeria, involves the burning of natural gases released during crude oil extraction due to inadequate infrastructure for harnessing them (Fawole et al., 2016; Anslem, 2013). This practice contributes significantly to air pollution, along with other illicit activities like oil theft and artisanal mining, releasing pollutants, particularly soot, into the atmosphere (Ahmed et al., 2024b; Orji et al., 2019). As rainwater traverses the atmosphere, it undergoes chemical alterations, incorporating pollutants like soot, trace elements, and heavy metals, thereby impacting its quality (Chen and Guo, 2022; Adeyeye et al., 2019).

The reliance on rain and surface water is emphasized by the prolonged wet seasons in this region, highlighting its critical role in supporting livelihoods (Ahmed et al., 2024b; Adejuwon, 2012). However, both surface and groundwater sources are susceptible to anthropogenic influences arising from activities such as overexploitation and pollution, necessitating urgent actions for environmental sustainability (Singh and Singh, 2017; Khatri and Tyagi, 2015). Understanding the hydrochemical composition of water resources is essential for evaluating their suitability for various purposes. Major ionic constituents, including SO_4^{2-}, HCO_3^-, Cl^-, Na^+, K^+, Ca^{2+}, and Mg^{2+}, along with physicochemical factors like pH, total dissolved solids (TDS), and electrical conductivity (EC), serve as vital indicators of water quality (Egbueri et al., 2019; Li et al., 2016). Moreover, the dynamic nature of water quality, shaped by atmospheric conditions, the hydrological cycle, and various geological and anthropogenic processes, underscores the complexity of water resource management (Ofgeha and Abshire, 2021; Ochelebe et al., 2020; Okorhi-Damisa et al., 2020).

Contrary to common perception, the presence of chemical and ionic constituents significantly influences water chemistry, necessitating a comprehensive understanding of factors affecting water quality, including their purity and spatial-temporal distribution (Liu et al., 2018; Akter et al., 2016). Numerous studies within the region have assessed water quality using methodologies such as the water quality index (WQI) model, potential ecological risks index (PERI), and heavy metals pollution index (HPI) to evaluate suitability based on physical, chemical, and metallic characteristics (Shankar, 2022; Abugu et al., 2021; Li et al., 2012). These environmental health and quality parameters provide comprehensive measures for assessing contamination levels in water bodies and the environment (Ahmed et al., 2024a; Chaniago and Taki, 2022). Monitoring these factors is crucial for evaluating water quality and environmental health (Bhardwaj et al., 2023; Olowoyo, 2011).

This study explores the intricate interplay of geospatial dispersion and distribution of major ions in rainwater and river water, coupled with the hydrochemical characterization of these water resources surrounding specific petroleum producing regions in South-Southern Nigeria, notably within the Obigbo Local Government Area (L.G.A) of Rivers State. By doing so, this research endeavors to advance our understanding of these complex dynamics and advocate for sustainable water resource management practices in areas impacted by petroleum production activities.

2. Methodology

2.1 Data Acquired and Analysis

2.1.1 Fieldwork and Sampling

The study involved a total of 41 water samples, consisting of 34 rainwater samples and 7 surface water samples. Rainwater was collected directly during precipitation using a purpose-built rainwater harvesting system. Prior to collection, all bottles were pre-sterilized. The rainwater was then transferred to 1.5-liter plastic water sampling containers. Additionally, surface water samples were obtained directly from rivers within the study area. The fieldwork was carried out by dividing the entire area into sub-regional locations categorized into five study axes: Obigbo, Komkom-Obiama, Okoloma, Egberu, and Umu Agbai-Obete (Table 1). Within these study axes, areas of settlements, markets, schools, hospitals, and petroleum facilities were mapped and sampled for rain and river water. The study area location mapping and geo-referencing of sampling points was achieved using the Garmin eTrex 32x, a rugged Handheld Global Positioning System (GPS).

2.1.2 Laboratory Analysis

The analysis of major ions in water samples involves several steps and methodologies to accurately determine the concentration of cations and anions present. For Calcium determination, a sample is initially diluted and treated with NaOH solution and an indicator to create a distinct color change. Then, the solution is titrated with EDTA solution until a distinct blue endpoint is reached. The volume of EDTA solution used allows for the calculation of Calcium carbonate ($CaCO_3$) content (Tiwari, et al., 2017). Magnesium content is calculated by difference in the volume of EDTA solution used for the calcium and the total volume required for hardness determination, with 1 mL of 0.01M EDTA equaling 0.2432 mg of magnesium. Sodium concentration is determined using a colorimetric method. This involves precipitating sodium and protein together, followed by a reaction with potassium ferrocyanide to produce a color change. The intensity of the color is measured photometrically, and the sodium concentration is inversely proportional to the color intensity (Egbueri et al., 2019).

Table 1. Rain and River Water Sampling Data

Sample		Study Axis	Reference Coordinates	
Type	**Numbers and Identification**		**Latitude (N)**	**Longitude (E)**
Rain	SN 1 (HSP 1), SN 2 (MKT 1), SN 3 (MKT 2), SN 4 (MKT 3), SN 5 (MKT 4), SN 6 (SCH 1), SN 7 (SCH 2), SN 8 (SET 10), SN 9 (FCLT 1)	**Obigbo**	4° 52' 41.7036"	7° 08' 44.7853"
River	SN 10 (RVR 1), SN 11 (RVR 2), SN 12 (RVR 3)			
Rain	SN 13 (MKT 5), SN 14 (SCH 3), SN 15 (SET 2), SN 16 (SET 3), SN 17 (SET 4)	**Komkom-Obiama**	4° 51' 22.8564"	7° 10' 56.0604"
River	SN 18 (RVR 4)			
Rain	SN 19 (MKT 6), SN 20 (MKT 7), SN 21 (SET 5), SN 22 (SET 6), SN 23 (SET 7), SN 24 (FCLT 2), SN 25 (FCLT 3)	**Okoloma**	4° 50' 40.2182"	7° 15' 12.6145"
River	SN 26 (RVR 5)			
Rain	SN 27 (HSP 2), SN 28 (MKT 8), SN 29 (SCH 4), SN 30 (SET 8), SN 31 (SET 9), SN 32 (SET 10)	**Egberu**	4° 50' 56.6016"	7° 19' 36.9012"
Rain	SN 33 (MKT 9), SN 34 (SET 11), SN 35 (SET 12), SN 36 (SET 13), SN 37 (SET 14), SN 38 (SET 15), SN 39 (SET 16)	**Umu Agbai-Obete**	4° 51' 12.3480"	7° 22' 38.5680"
River	SN 40 (RVR 6), SN 41 (RVR 7)			

Nitrate concentration is determined through a Cadmium reduction method using a multi-parameter bench photometer, where the sample is treated with a specific reagent and analyzed at a particular wavelength. Chloride concentration is determined via argentometric titration, where the sample is titrated against a standard solution of silver nitrate until brick red precipitates form, with the volume of titrant used allowing for the calculation of chloride concentration. Bicarbonate concentration is determined by titration with standard HCl after precipitating carbonate with Barium Chloride, with the volume of acid used allowing for the calculation of bicarbonate concentration. Sulphate concentration is determined by precipitating with Barium chloride, filtering, drying, and weighing the precipitate, with the weight of the precipitate allowing for the calculation of sulphate concentration (Appelo and Postma, 1993). Each of these procedures provides detailed steps to follow to accurately determine the concentration of specific ions in water samples, enabling comprehensive analysis of water quality and composition.

2.1.3 Hydrochemical and Geospatial Modelling

This study employs the Piper Diagram, Durov Diagram, and Schoeller Diagram for hydrochemical modelling. The primary objective of these techniques is to identify chemical relationships between water samples. Similar chemical characteristics often indicate similar hydrologic histories, recharge areas, infiltration pathways, and flow paths in terms of climate, mineralogy, and residence time (Tiwari et al., 2017). The Piper diagram's graphical representation illustrates the chemistry of water samples using separate ternary plots for cations and anions. The apexes of the cation plot represent calcium, magnesium, sodium, and potassium cations, while the apexes of the anion plot represent sulfate, chloride, carbonate, and bicarbonate anions (Piper, 1944). The two ternary plots are projected into a diamond, allowing for the classification of waters by hydrochemical facies. The Piper diagram is useful for identifying water mixing and tracking changes over space and time, but it has limitations such as renormalized concentrations and difficulty accommodating other significant cations or anions (Ochelebe and Kudamnya, 2022; Piper, 1944).

The Schoeller diagram is a semi-logarithmic representation of the concentration of major ionic constituents in water, including sulfate (SO4), bicarbonate (HCO3), magnesium (Mg), calcium (Ca), and sodium/potassium (Na/K), and in equivalent per million per kg of solution (meg/kg). This diagram allows for the representation of major ions from multiple samples on a single graph, facilitating the discrimination of samples with similar patterns (Schoeller, 1967). The Durov diagram in AquaChem serves as an alternative to the Piper diagram. It plots major ions as percentages of mill-equivalents in two base triangles, with total cations and anions set equal to 100% (Durov, 1948). Data points in the triangles are projected onto a square grid, revealing clustering of data points to indicate samples with similar compositions. The Durov diagram is particularly useful for analyzing large sample groups (Ochelebe and Kudamnya, 2022).

The geospatial modelling involved the spatial representation and distribution of the Major Ions (Cations and Anions) concentrations at each location using ArcGIS 10.4 software, and Microsoft Excel, integrating the ionic laboratory analysis results from both rain and river water samples. The software processed these data as input variables, employing algorithms to generate graphical representations such as curves or contours (Ahmed and Taiwo, 2023), effectively illustrating the spatial distribution of water pollutant levels in the studied region (Shankar, et al., 2022).

2.2 Study Area

The study area encompasses Oyigbo Local Government Area (L.G.A.), situated in Rivers State, South-Southern Nigeria. Positioned approximately 30 kilometers northeast of Port Harcourt, Oyigbo falls within the geographic coordinates of latitude 4˚54' to 4˚46' N and longitude 7˚15' to 7˚25' W, covering a total area of 248.00 km² (95.75 sq mi) (Figure 1). Oyigbo has its administrative headquarters located in Afam, and shares boundaries with Khana to the Southeast, Tai to the South, Eleme and Obio/Akpor to the Southwest, while its Northern boundary abuts Abia State (NBS, 2006). The area is inhabited primarily by the Asa and Ndoki people. Oyigbo plays a significant role in the sociopolitical and economic dynamics of

Rivers State, contributing to the diverse cultural and environmental tapestry of the Niger Delta region.

Population trends over the years indicate significant growth from 40,407 in 1975 to 125,666 in 2015, accompanied by an increase in population density (NBS, 2006). The demographic dynamics of the Oyigbo area are intricately linked to the abundance of dry land and the unique terrain of the region (Samuel et al., 2022).

Oyigbo area experiences a tropical wet climate, with prolonged and intense rainy seasons and brief dry seasons. The dry season occurs from November to February, with December being the driest month. The area receives heavy precipitation in September, with an average rainfall of 370 mm (Onwuka et al., 2021). Temperature variations are minimal, with average temperatures ranging from 25°C to 28°C throughout the year. Relative humidity is high, averaging around 80 percent during the rainy season and dropping to roughly 40 percent in the dry season.

Situated in the equatorial rainforest belt of Nigeria, Oyigbo experiences an annual mean rainfall of about 2500 mm, with the majority occurring between May and October. The vegetation consists mainly of tropical rainforest, particularly along the river systems, and secondary bushes resulting from farming or fallowing (Onwuka et al., 2021).

The study area serves as a prominent oil-producing region and a major industrial center, hosting multinational firms, especially those involved in the petroleum industry. Rapid population growth is fueled by affordable housing relative to Port Harcourt, leading to heavy traffic as workers commute to the city (Samuel et al., 2022). The discovery of crude oil has transformed the area's economy, with significant petroleum facilities such as the Afam Power Station, Shell Okoloma Gas Plant, and Nigerian Gas Plant Plc driving revenue generation. These facilities, while vital to the local economy, also pose environmental challenges that require careful management.

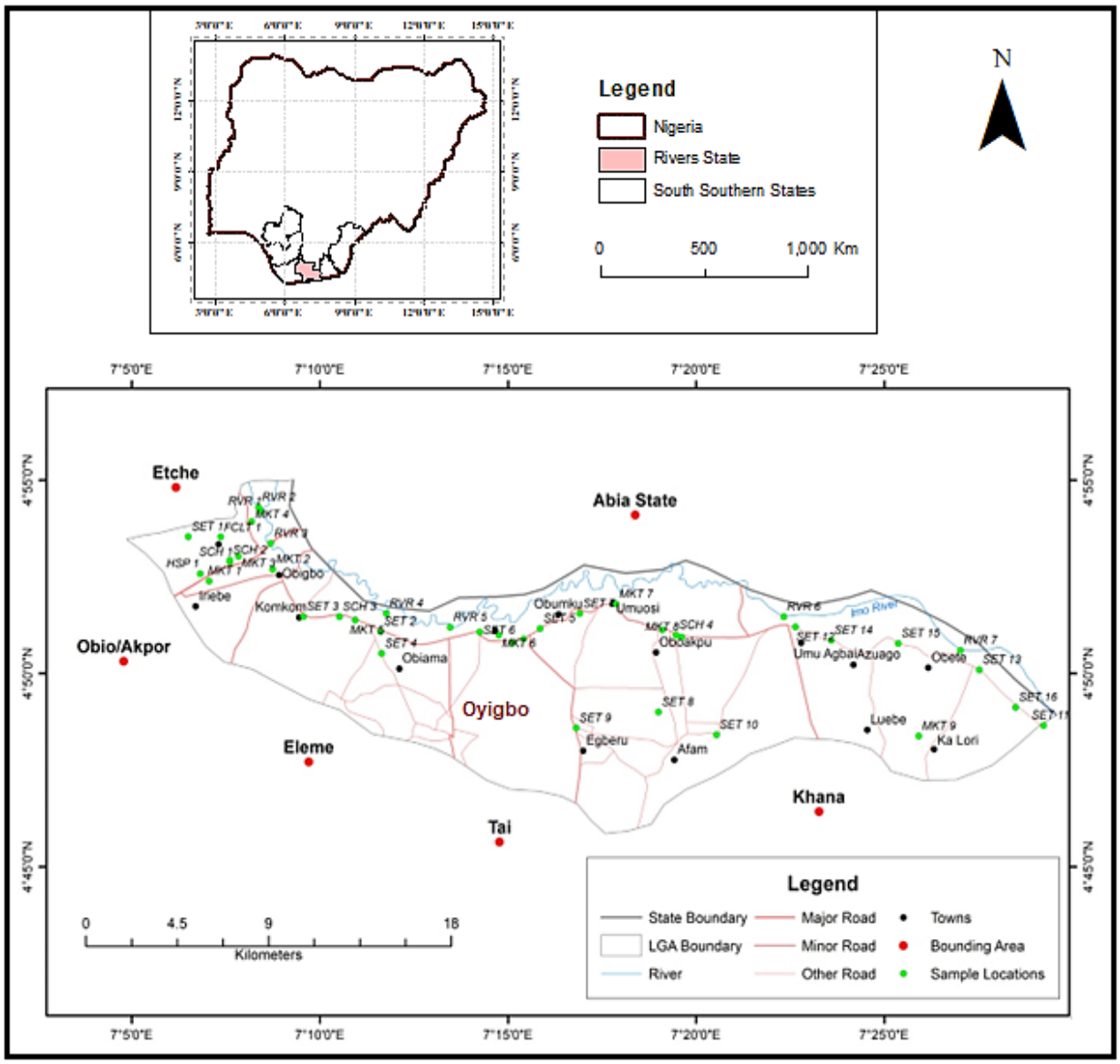

Fig 1. Map Showing Nigeria, South Southern States, Rivers State, Study Area, Locations and Sampling Points (*Source: Digitized by Author*)

3. Results and Discussions

Major ions, essential components in environmental chemistry, are introduced into the environment through two primary avenues: natural processes and anthropogenic activities. Natural occurrences involve cations, such as calcium or magnesium, dissolving due to the weathering of minerals found in rocks (Khatri and Tyagi, 2015). Conversely, anthropogenic sources stem from human activities, including industrial operations, vehicular emissions from roads, and mining activities, which can lead to contamination by cationic pollutants (Chen and Guo, 2022). The presence of cations and anions in water holds profound physiological significance, particularly for living organisms, including humans (Li et al., 2016).

Elements like calcium, magnesium, copper, and iron play pivotal roles in various biological processes, such as oxygen transport within the body (Ahmed et al., 2024a). Quantifying cationic and anionic concentrations in water samples provides valuable insights into environmental dynamics. Table 2a presents the concentrations, measured in milligrams per liter (mg/L), of cations and anions in rainwater, shedding light on natural and anthropogenic atmospheric deposition processes. Meanwhile, Table 2b displays corresponding concentrations for river water samples collected within the study area, offering critical data on the environmental quality and potential anthropogenic impacts on water bodies.

Table 2a. Concentrations of Cations and Anions for Rainwater (mg/L)

	Ca	Mg	Na	K	HCO_3	Cl	SO_4	NO_3
Max	4.02	1.12	1.89	1.75	2.13	2.11	3.91	1.22
Min	0.02	0.01	0.08	0.07	0.21	0.07	0.08	0.001
Mean	1.51	0.34	1.05	0.89	1.32	1.03	1.59	0.26

Table 2b. Concentrations of Cations and Anions for River Water (mg/L)

	Ca	Mg	Na	K	HCO_3	Cl	SO_4	NO_3
Max	28.71	23.21	31.05	26.99	29.85	34.92	31.29	39.72
Min	12.16	12.37	14.93	14.63	15.71	22.63	17.18	15.12
Mean	20.5	17.62	20.59	22.08	22.23	27.99	24.6	26.47

3.1 Geospatial Distribution of Cations and Anions

3.1.1 Cations

The distribution of cation concentrations across the study area is depicted in Figure 2a-e, illustrating the percentage spreading of cations in both rain and river water samples. In Figure 2a, the cation percentage spreading is portrayed for the Obigbo Axis, while Figure 2b showcases the distribution in the Komkom-Obiama Axis. Similarly, Figure 2c illustrates the percentage spreading of cations in the Okoloma Axis, while Figure 2d provides insight into the Egberu Axis's cation distribution. Lastly, Figure 2e offers a depiction of the percentage spreading of cations in the Umu Agbai-Obete Axis.

In the **Obigbo axis**, analysis reveals that river samples exhibit the highest percentage of cation spreading across the sampled 12 locations. Calcium (Ca) concentrations are notably highest in locations SN 12 (RVR 3), SN 10 (RVR 1), and SN 11 (RVR 2), accounting for 36%, 23%, and 19% respectively, contributing to 78% (over three-quarter) of the total Ca spreading across the axis. The remaining nine samples represent less than one-quarter, with SN 8 (SET 1) covering 5%, SN 7 (SCH 2) with 4%, and SN 2, SN 4 (MKT 1, and MKT 3), and other locations contributing 2% or less. Similarly, Magnesium (Mg) are prominently distributed in RVR 3, RVR 2, and RVR 1, constituting 42%, 32%, and 23% respectively, representing 97% of the total Mg concentrations in the axis. SN 5 (MKT 4) accounts for 2%, while the remaining eight samples each contribute 1% or less. Sodium (Na) also demonstrate comparable trends, with RVR 3, RVR 2, and RVR 1 collectively covering 85% of the total area. Other samples, such as SN 2 (MKT 1), SN 5 (MKT 4), SN 6 (SCH 1), and SN 8 (SET 1), each represent 2%, while SN 9 (FCLT 1) accounts for 3%. Potassium (K) concentrations mirror similar trends, with RVR 3, RVR 2, and RVR 1 dominating at 90% coverage. Other samples, such as SN 3 (MKT 2), SN 6 (SCH 1), SN 7 (SCH 2), and SN 8 (SET 1), each contribute 2%, while the remaining samples represent 1% or less.

In the **Komkom-Obiama axis** of the study area, a distinct pattern emerges in the distribution of cations across the six sampled locations. Notably, location SN 18 (RVR 4) stands out with the highest percentage of cation spreading. Calcium (Ca) predominates in this location, covering slightly over half of the study area at 56%. In contrast, the remaining five samples collectively represent less than half, with SN 16 (SET 3) accounting for 14%, SN 13 (MKT 5) at 10%, SN 15 (SET 2) with 9%, and SN 14 (SCH 3) contributing 7%. Similarly, magnesium (Mg) concentrations peak in SN 18 (RVR 4), occupying a substantial 97% of the total Mg concentrations in the Komkom-Obiama axis. SN 14 (SCH 3), SN 15 (SET 2), and SN 17 (SET 4) each contribute 1%, while SN 13 (MKT 5) and SN 16 (SET 3) samples each represent less than 1%. Sodium (Na) exhibits a comparable distribution pattern, with RVR 4 (SN 18) capturing the highest percentage spreading at 84%. SN 16 (SET 3) represents 6%, while SN 15 (SET 2) and SN 17 (SET 4) each contribute 4%. SN 13 (MKT 5) accounts for 2%, and SN 14 falls below 1%. Similarly, potassium (K) concentrations follow a similar trend, with RVR 4 (SN 18) dominating at 81% coverage. SN 14 (SCH 3), SN 13 (MKT 5), SN 16 (SET 3), and SN 15 (SET 2) contribute 7%, 6%, 5%, and 1%, respectively, while SN 17 (SET 4) accounts for less than 1%.

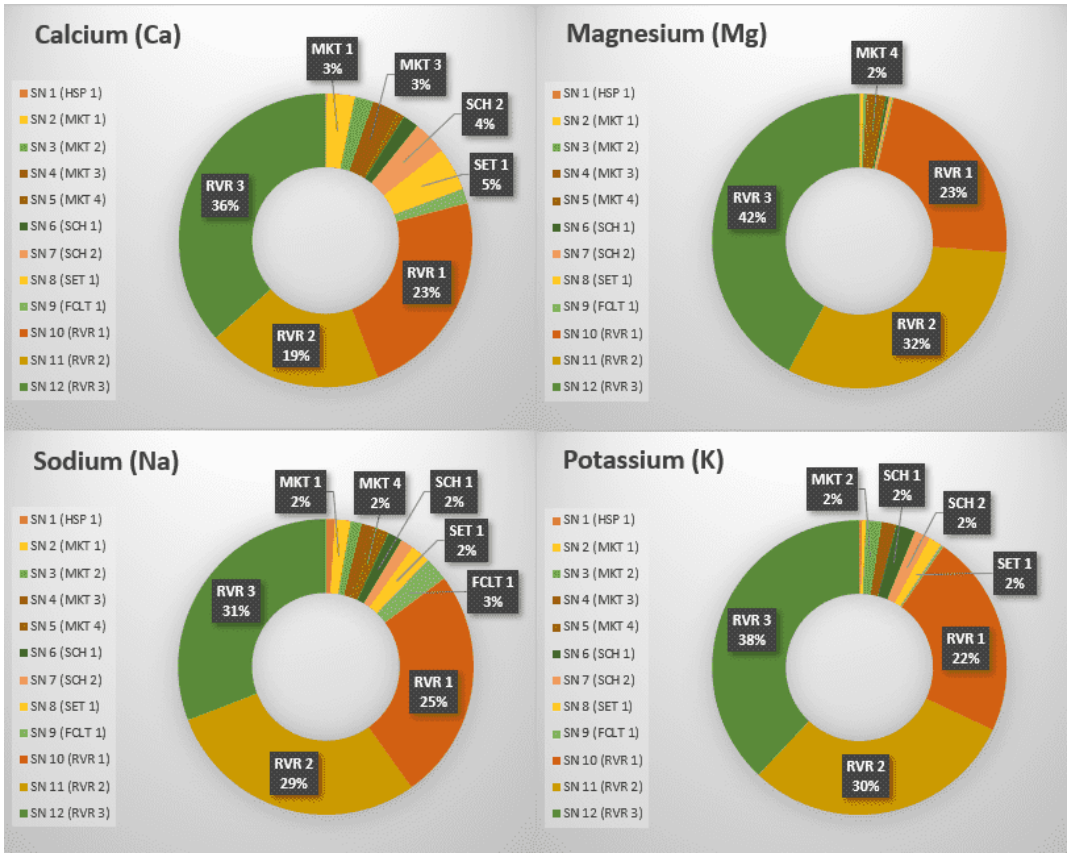

Fig 2a. Percentage Spreading of Cations in Obigbo Axis

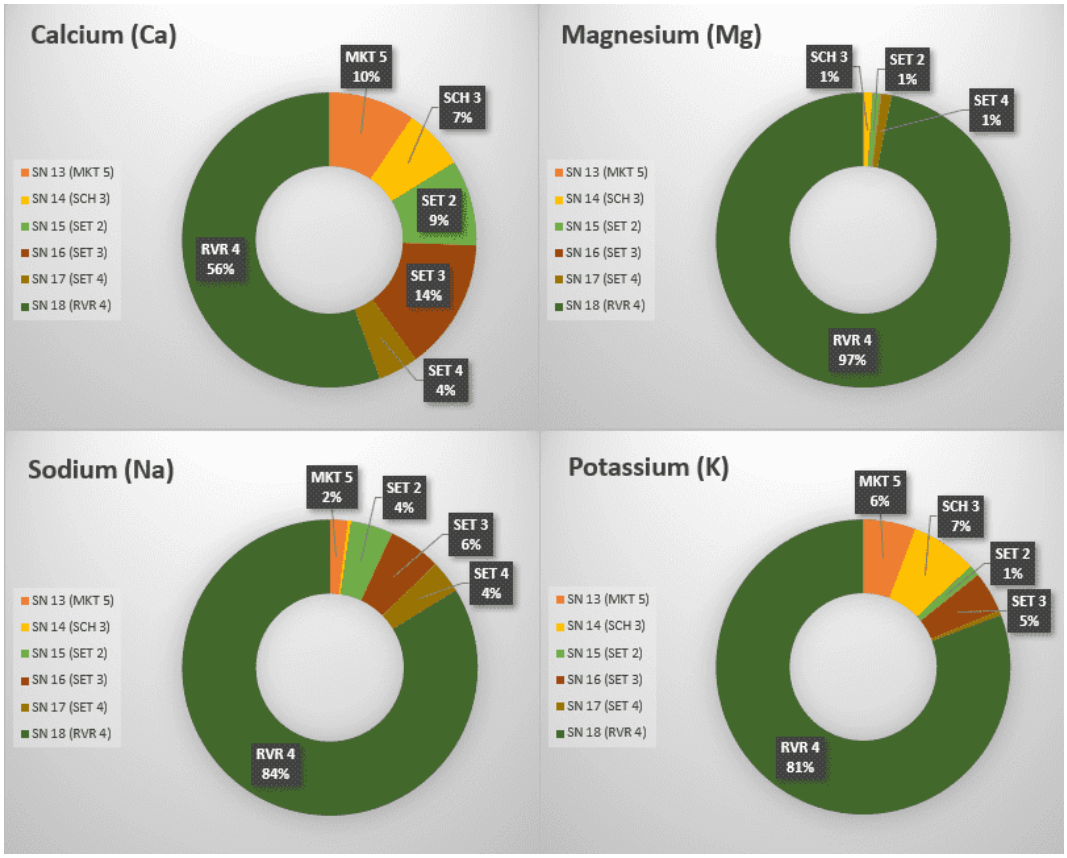

Fig 2b. Percentage Spreading of Cations in Komkom-Obiama Axis

In the **Okoloma study axis**, a consistent pattern emerges with location SN 26 (RVR 5) exhibiting the highest percentage of cations spreading across the sampled eight locations. Calcium (Ca) is notably prominent in this location, covering three-quarters of the study area at 76%. Conversely, the remaining seven samples collectively represent one-quarter, with SN 22 (SET 6) occupying 11%, SN 19 (MKT 6) at 5%, and SN 24 (FCLT 2) and SN 25 (FCLT 3) each contributing 3%. SN 20 (MKT 7), SN 21 (SET 5), and SN 23 (SET 7) collectively account for 2% and less. Similarly, magnesium (Mg) concentrations peak in SN 26 (RVR 5), occupying a significant 87% of the entire Mg concentrations in the Okoloma study axis. SN 20 (MKT 7) and SN 24 (FCLT 2) each contribute 4%, while SN 19 (MKT 6) and SN 23 (SET 7) represent less than 3% and 2%, respectively, with the remaining samples contributing less than 2%. Sodium (Na) also displays a predominant distribution at SN 26 (RVR 5), covering over three-quarters of the area at 83%. SN 25 (FCLT 3) represents 5%, while the remaining sample locations contribute 3%, 2%, and 1%, respectively. Similarly, potassium (K) concentrations mirror this trend, with RVR 5 (SN 26) dominating at 80% coverage. SN 20 (MKT 7) occupies less than 1%, MKT 6 and SET 7 each contribute 4%, while SET 5, SET 6, FCLT 2, and FCLT 3 samples represent 3% each.

In the **Egberu axis** of the study area, a discernible distribution pattern emerges across the six sampled locations concerning cation concentrations. Calcium (Ca) exhibits notable variations across these locations, with SN 32 (SET 10) occupying the highest percentage at 39%. This is followed by SN 30 (SET 8) at 22%, SN 31 (SET 9) at 14%, SN 27 (HSP 2) at 10%, SN 28 (MKT 8) at 8%, and SN 29 (SCH 4) at 7%. Magnesium (Mg) concentrations peak at SN 30 (SET 8), representing 30% of the total, followed by SN 28 (MKT 8) and SN 31 (SET 9) at 21% each. SN 32 (SET 10) follows closely at 19%, with SN 29 (SCH 4) contributing 8% and SN 27 (HSP 2) representing 1%. Sodium (Na) displays a similar distribution pattern to Mg, with SN 30 (SET 8) holding the highest percentage at 28%. SN 29 (SCH 4) closely follows at 23%, while SN 28 (MKT 8) accounts for 18%. SN 32 (SET 10) occupies 16%, SN 31 (SET 9) 14%, and SN 27 (HSP 2) represents 1%. In terms of potassium (K) concentrations, SN 29 (SCH 4) dominates with 29%, trailed by SN 27 (HSP 2) at 19%, SN 28 (MKT 8) at 18%, SN 31 (SET 9) at 17%, and SN 32 (SET 10) at 16%. SN 30 (SET 8) exhibits the lowest percentage, representing only 1% of the total.

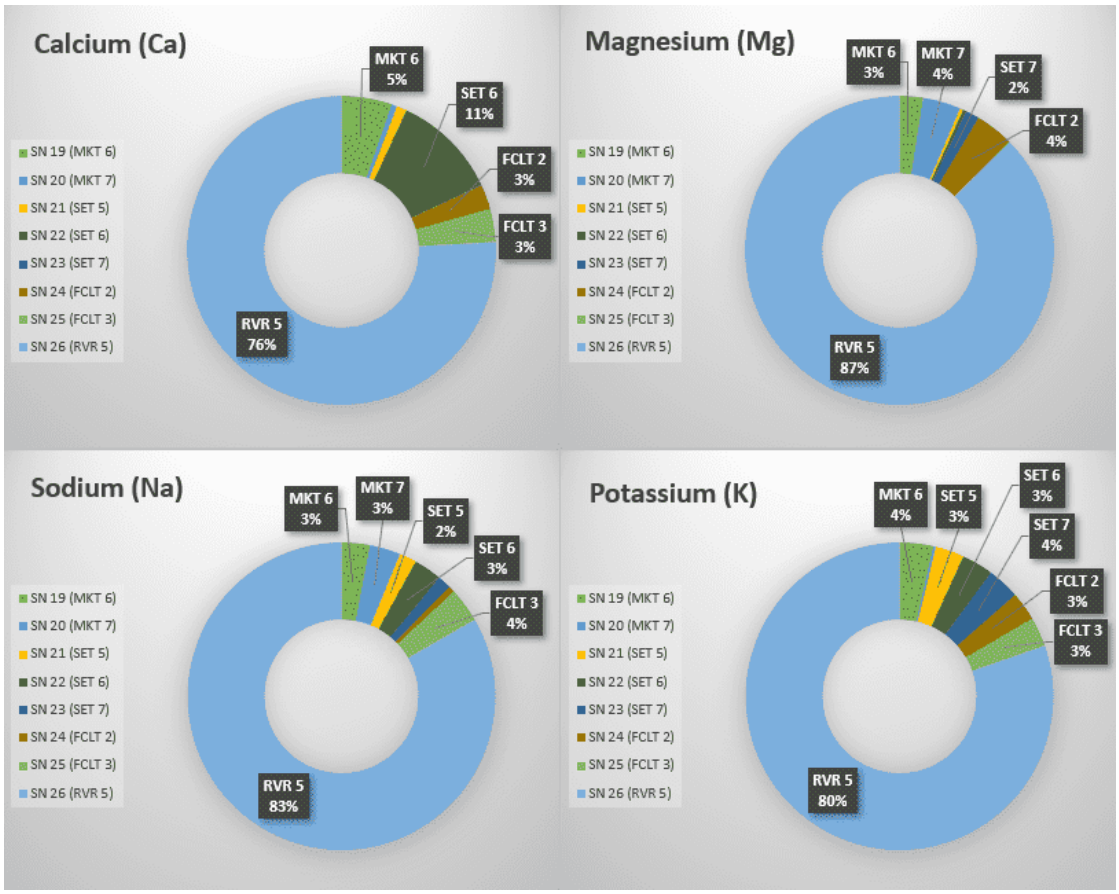

Fig 2c. Percentage Spreading of Cations in Okoloma Axis

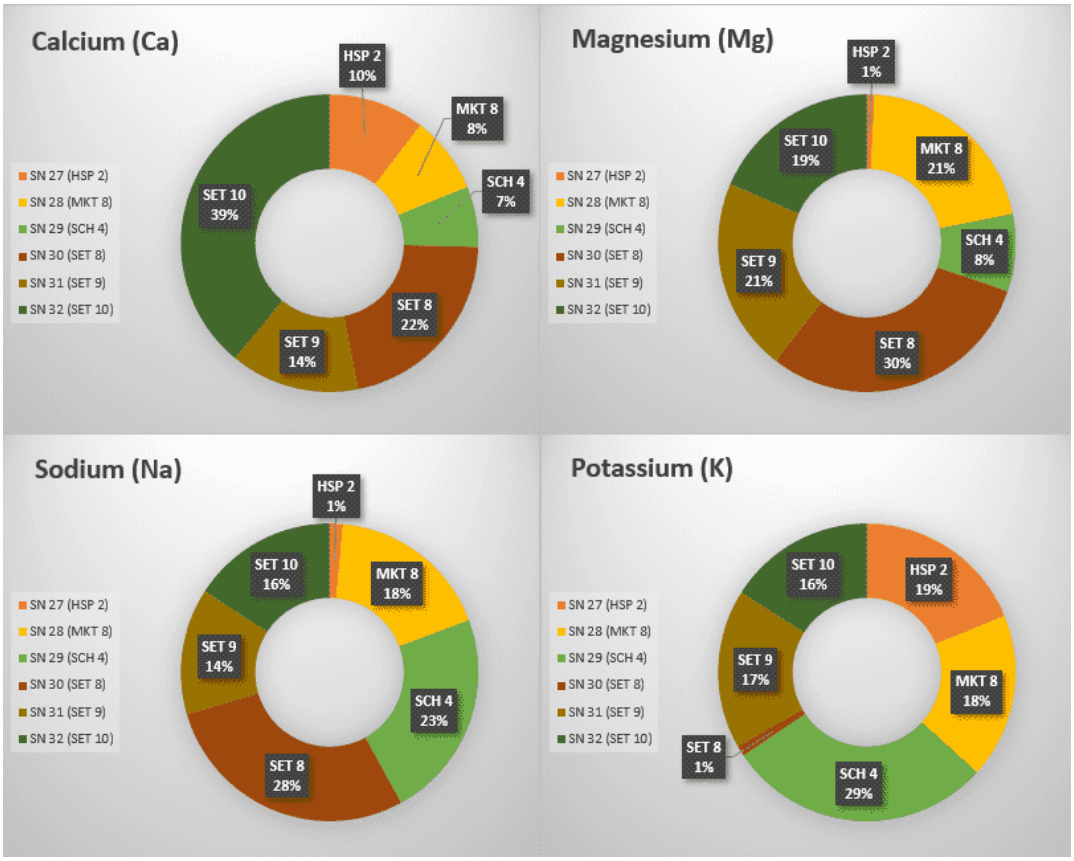

Fig 2d. Percentage Spreading of Cations in Egberu Axis

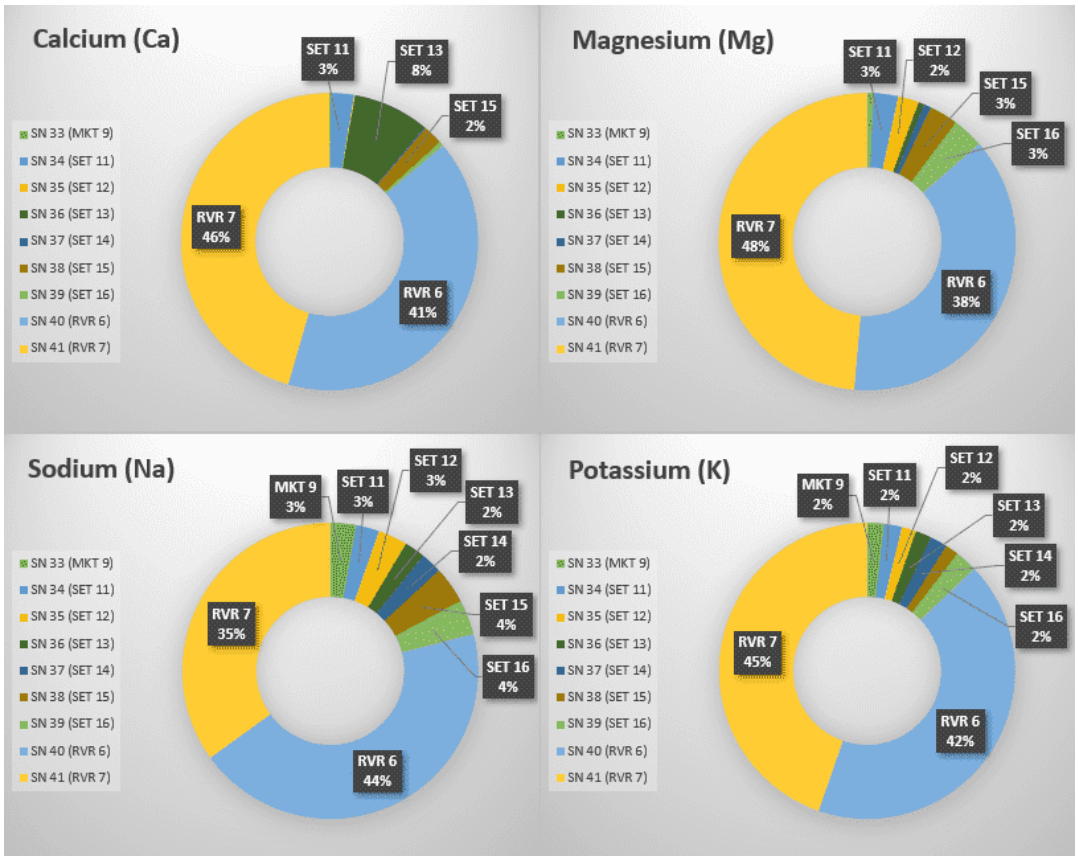

Fig 2e. Percentage Spreading of Cations in Umu Agbai-Obete Axis

A consistent distribution pattern is evident in the **Umu Agbai-Obete axis**, with locations SN 40 (RVR 6) and SN 41 (RVR 7) emerging as the primary contributors to cation spreading across the nine sampled locations. Calcium (Ca) concentrations are notably high in these two locations covering 87% of the area. SN 41 (RVR 7) accounts for 46%, while SN 40 (RVR 6) represents 41%. The remaining seven samples collectively contribute less than one-quarter, with SN 36 (SET 13) occupying 8%, SN 34 (SET 11) at 3%, and SN 38 (SET 15) at 2%. SN 33 (MKT 9), SN 35 (SET 12), SN 37 (SET 14), and SN 39 (SET 16) account for less than 2%. Magnesium (Mg) concentrations peak at SN 41 (RVR 7) with 48% and SN 40 (RVR 6) with 38%. SN 34 (SET 11), SN 38 (SET 15), and SN 39 (SET 16) each represent 3%, while SN 35 (SET 12) accounts for 2%. Sodium (Na) also exhibits a predominant distribution, with SN 40 (RVR 6) at 44% and SN 41 (RVR 7) at 35%. SET 15 and SET 16 each represent 4%, while MKT 9, SET 11, and SET 12 each contribute 3%. SET 13 and SET 14 each represent 2%. Regarding potassium (K) concentrations, SN 41 (RVR 7) and SN 40 (RVR 6) dominate at 45% and 42%, respectively. SET 9, SET 11, SET 12, SET 13, SET 14, and SET 16 each occupy 2%, while SET 15 represents less than 1%.

The spatial distribution of cations is reflective of the percentage spreading analysis of the Ca, Mg, Na, and K abundance which demonstrates a relatively uniform pattern across the study area. While rainwater samples exhibit limited variation, higher concentrations are notable along the river channel, particularly in the upper region of Oyigbo (Figure 3). This suggests a pronounced concentration within the river system compared to rainwater, where concentrations are relatively lower. The spatial distribution of cations in rainwater displays a discernible concentration, indicated by color variations, notably higher in the eastern and western central regions of the study area. These areas correspond to locations adjacent to petroleum activities or production facilities. In general, geospatial analysis reveals consistent concentration levels of major cations throughout the Oyigbo area, indicating minimal variability across the region. This uniformity hints at a relatively stable environmental condition regarding cationic presence. Crucially, all measured concentrations adhere to the standards set by the World Health Organization (WHO, 2017), highlighting environmentally acceptable levels of cations within the area.

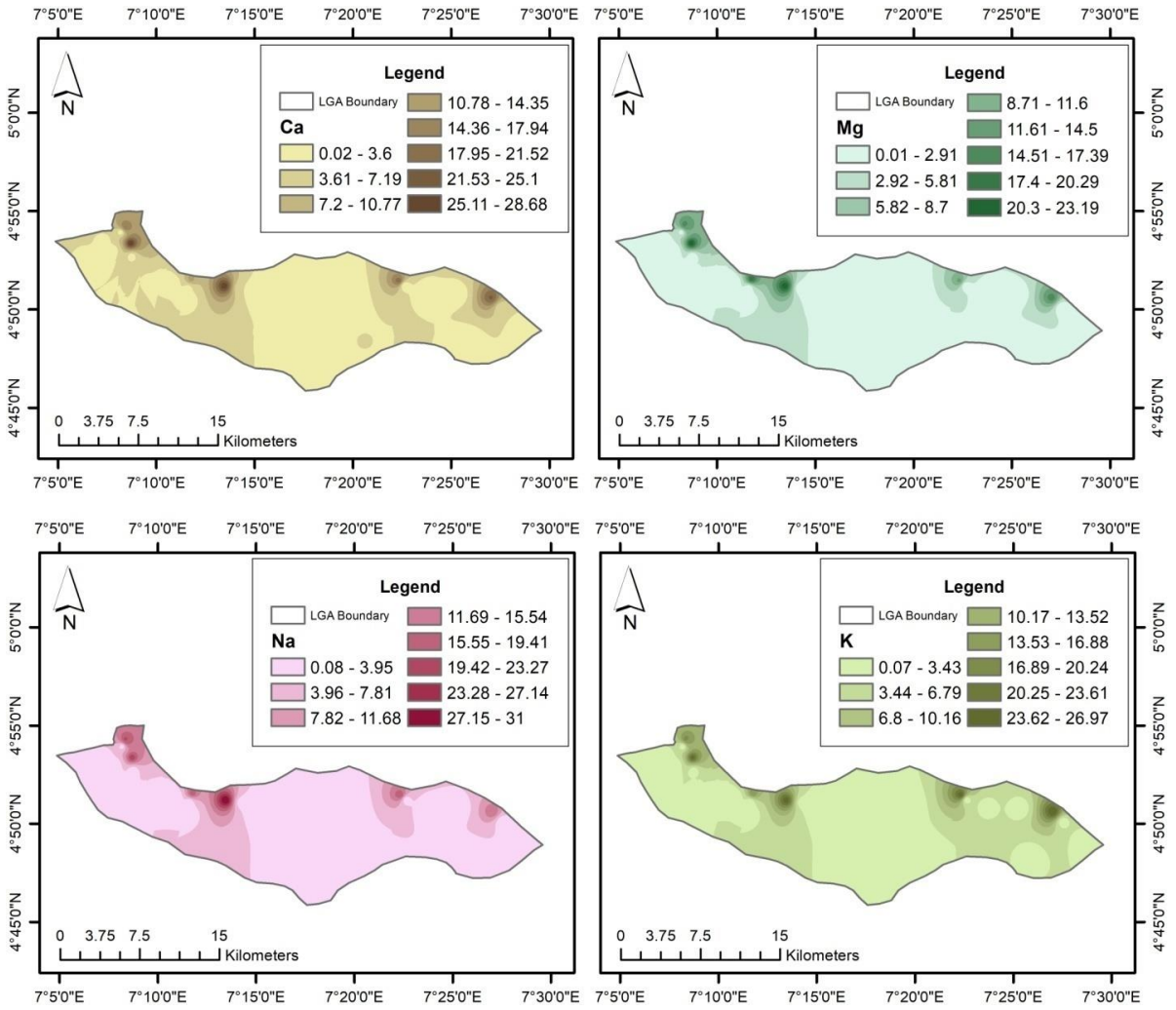

Fig 3. Geospatial Dispersion Maps of Cations across the Study Area

3.1.2 Anions

Figure 4a-e presents the distribution of anion concentrations across the study area, depicting the percentage spreading of anions in both rain and river water samples. Specifically, Figure 4a illustrates the anion percentage spreading in the Obigbo Axis, while Figure 4b highlights the distribution in the Komkom-Obiama Axis. Similarly, Figure 4c showcases the percentage spreading of anions in the Okoloma Axis, and Figure 4d provides insights into the Egberu Axis's anion distribution. Lastly, Figure 4e offers a depiction of the percentage spreading of anions in the Umu Agbai-Obete Axis. These figures collectively offer a comprehensive overview of the spatial distribution of anion concentrations across various axes within the study area.

Analysis conducted in the **Obigbo axis** reveals that river samples exhibit the highest percentage of anion spreading across the sampled 12 locations. Notably, Bicarbonate (HCO3) concentrations are most prominent in locations SN 12 (RVR 3), SN 10 (RVR 1), and SN 11 (RVR 2), constituting 32%, 27%, and 24% respectively.

These locations collectively contribute to 83% (over three-quarters) of the total HCO3 spreading across the axis. In contrast, sample locations SN 1 (HSP 1), SN 2 (MKT 1), SN 4 (MKT 3), SN 6 (SCH 1), SN 7 (SCH 2), and SN 9 (FCLT 1) each account for 2% of the total, while SN 5 (MKT 4) occupies 3%. The remaining two locations contribute 1% and below. Similarly, Chloride (Cl) is prominently distributed in RVR 3, RVR 1, and RVR 2, constituting 32%, 30%, and 27% respectively, representing 89% of the total Cl concentrations in the axis. SN 5 (MKT 4) and SN 8 (SET 1) account for 3% and 2% respectively, while the remaining eight samples each contribute 1% or less. Sulphate (SO4) also demonstrates comparable trends, with RVR 3, RVR 1, and RVR 2 collectively covering 79% of the total area. Other samples, such as SN 2 (MKT 1), SN 4 (MKT 3), and SN 9 (FCLT 1), account for 4% each, while SN 3 (MKT 2) and SN 7 (SCH 2) represent 3% and 2% respectively. Nitrate (NO3) reflects RVR 2, RVR 1, and RVR 3 dominating at 95% coverage, while the remaining samples contribute 2% and below.

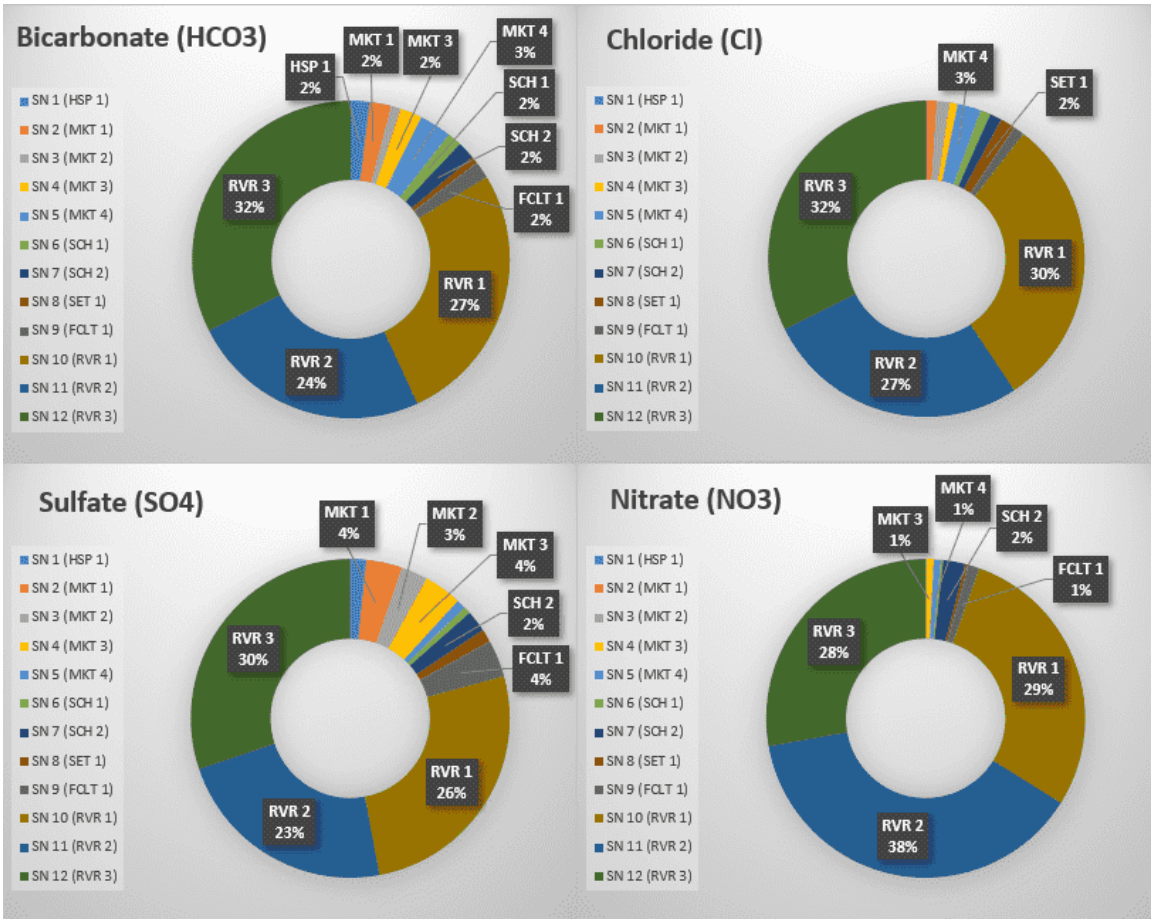

Fig 4a. Percentage Spreading of Anions in Obigbo Axis

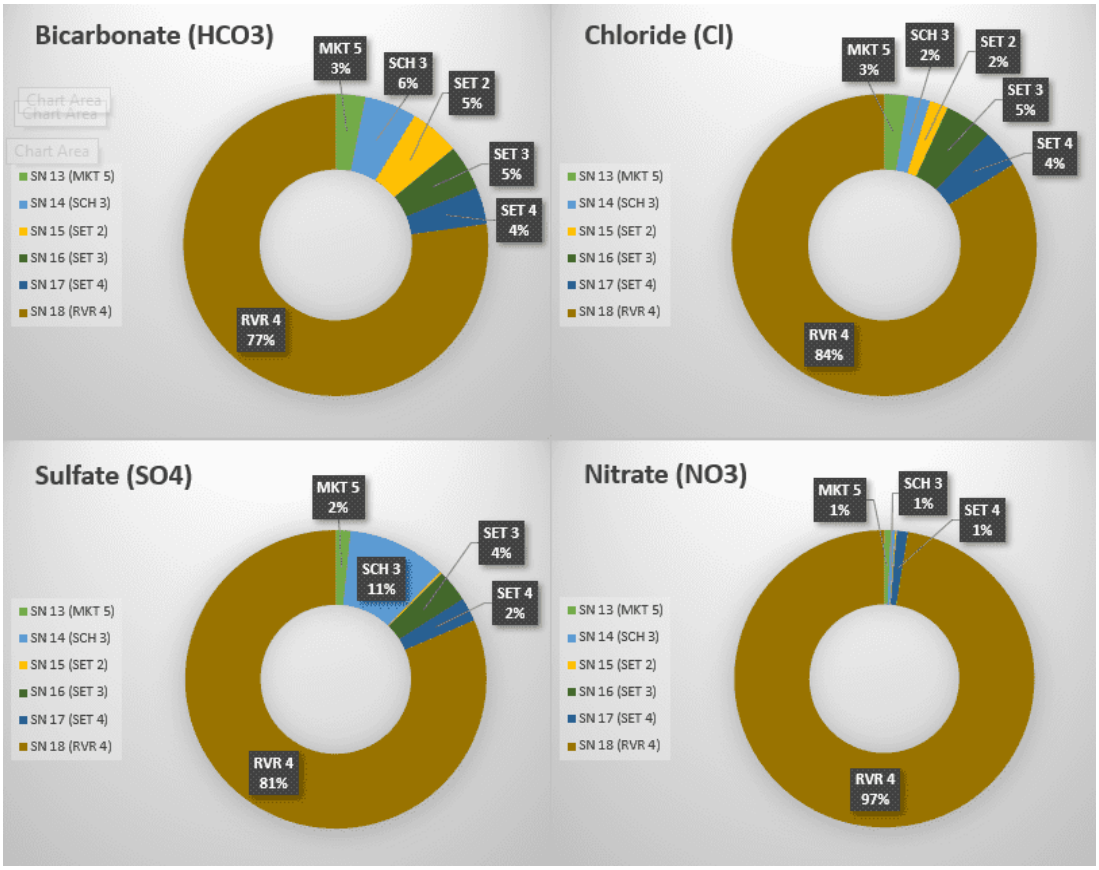

Fig 4b. Percentage Spreading of Anions in Komkom-Obiama Axis

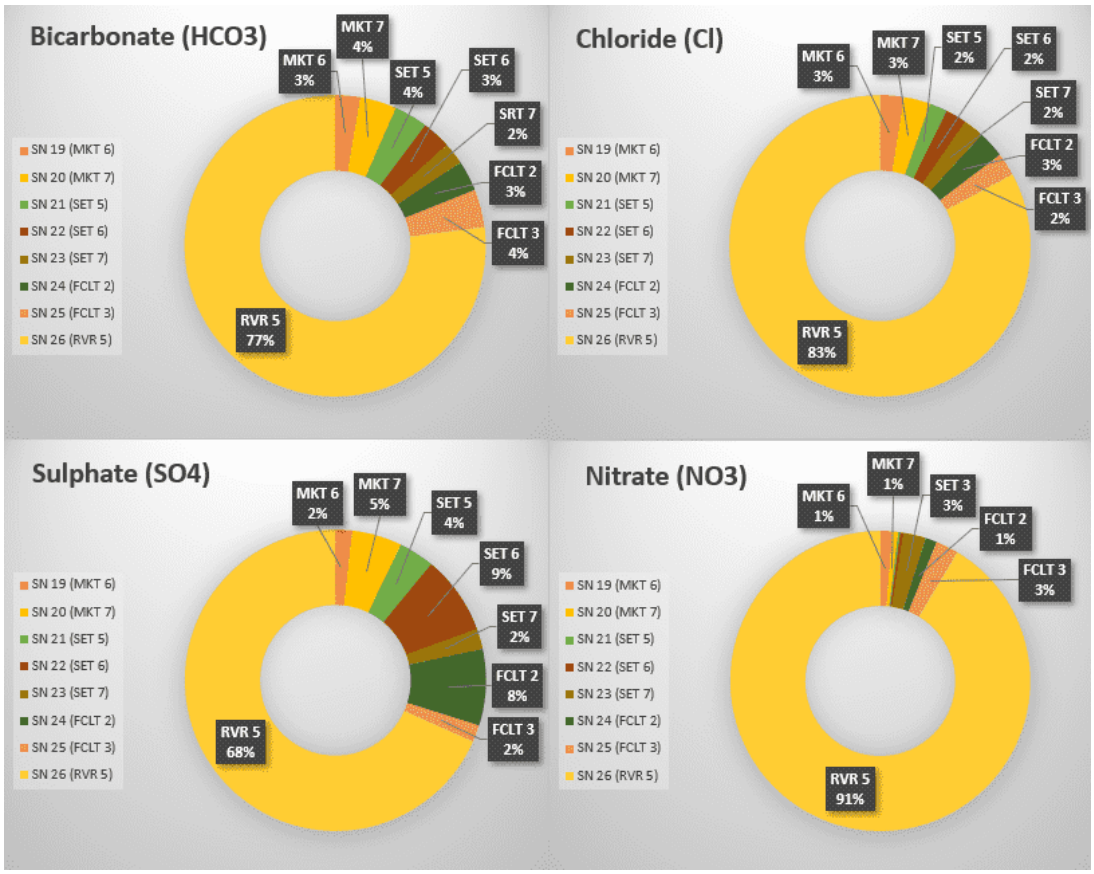

Fig 4c. Percentage Spreading of Anions in Okoloma Axis

In the **Komkom-Obiama axis** of the study area, a distinct pattern emerges in the distribution of anions across the six sampled locations. Notably, location SN 18 (RVR 4) stands out with the highest percentage of anion spreading, particularly with HCO3 concentrations covering three-quarters at 77%. In contrast, the remaining five samples collectively represent less than one-quarter, contributing 6%, 5%, 4%, and 3% each. Similarly, Cl concentrations peak in SN 18 (RVR 4), occupying 84%. Samples SN 14 (SCH 3), SN 15 (SET 2), SN 17 (SET 4), SN 13 (MKT 5), and SN 16 (SET 3) each represent 5% and below. SO4 exhibits a comparable distribution pattern, with RVR 4 (SN 18) capturing the highest percentage spreading at 81%. SN 14 (SCH 3) represents 11%, while the remaining samples each contribute 4% and below. NO3 concentrations show the highest coverage with RVR 4 (SN 18) at 97%, while the rest samples account for 1% and less.

In the **Okoloma study axis**, a consistent pattern of location SN 26 (RVR 5) having the highest percentage of anion spreading across all eight locations is displayed. This includes 91% NO3, 83% Cl, 77% HCO3, and 68% SO4 representations. Notable locations within the community include SN 20 (MKT 7), contributing 4% HCO3, 3% Cl, 5% SO4, and 1% NO3. Additionally, SN 22 (SET 6), SN 24 (FCLT 2), and SN 25 (FCLT 3) also make substantial contributions within the rainwater sampled locations across the Okoloma study axis.

Of note is the higher percentage spread for Sulphate, with SET 6 and FCLT 2 representing 9% and 8% respectively. Conversely, the lowest distribution and percentage spreading are observed with SET 3 and FCLT 3, each accounting for 3%, while the remaining anions are at 1%. This distribution pattern underscores the prevalence of Nitrates across all the rainwater samples within this axis compared to other anions.

In the **Egberu axis** of the study area, a distinct distribution pattern emerges across the six sampled locations concerning anion concentrations. Bicarbonate (HCO3) exhibits notably balanced variations across these locations, with SN 31 (SET 9), SN 28 (MKT 8), and SN 29 (SCH 4) each representing 19% of the distribution. SN 32 (SET 10) and SN 30 (SET 8) follow closely, accounting for 17% and 16% respectively, while SN 27 (HSP 2) occupies 10%. Similarly, Chloride (Cl) and Sulfate (SO4) spread across the Egberu study axis with only slight variations in concentrations. However, a higher dominance of Nitrate is noticeable at locations SN 27 and SN 31, occupying 47% and 31% respectively, with HSP 2 and SET 9. This is followed by SCH 4 at location SN 29, accounting for 14%. The remaining three locations, MKT 8, SET 8, and SET 10, represent 4%, 3%, and 1% respectively of the NO3 distribution across the Egberu study axis.

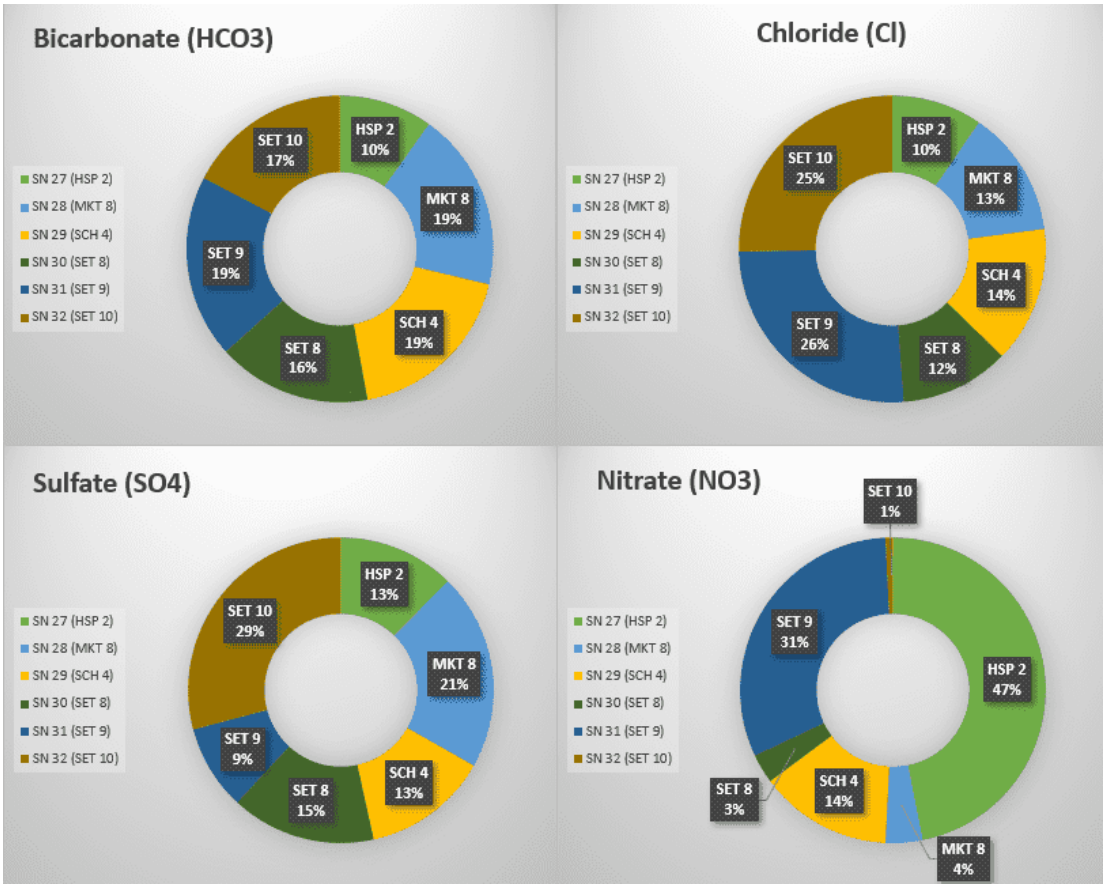

Fig 4d. Percentage Spreading of Anions in Egberu Axis

In the **Umu Agbai-Obete axis**, a consistent distribution pattern emerges, with locations SN 40 (RVR 6) and SN 41 (RVR 7) being the primary contributors to anion spreading across the nine sampled locations. Bicarbonate (HCO3) concentrations are notably high in these two locations, covering 88% of the area. SN 41 (RVR 7) accounts for 48%, while SN 40 (RVR 6) represents 40%. The remaining seven samples collectively contribute less than one-quarter, with SN 37 (SET 14) occupying 3%, while the rest account for 2% each, except for SN 38 (SET 15) at 1%, and SN 35 (SET 12) falling below 1%. Chloride (Cl) and Sulphate (SO4) concentrations also peak at SN 41 (RVR 7) and SN 40 (RVR 6), displaying similar trends of anion distributions and spreading as HCO3 across the Umu Agbai-Obete study axis. However, in the case of Sodium (Na), distribution by locations is minimal, with almost the entire spread coming from RVR 7 and RVR 6, which combinedly account for 98%, leaving only 2% for SET 13 at location SN 36. The remaining six sampled locations represent 5% of the overall Nitrate distribution within the Umu Agbai-Obete study axis.

The spatial distribution of anions mirrors the percentage spreading analysis of the abundance of NO3-, Cl-, HCO3-, and SO42-, exhibiting a relatively uniform pattern across the study area. While rainwater samples show limited variation, higher concentrations, or hotspots, are observed along the river channel, particularly in the upper region of Oyigbo (Figure 5). This suggests potential localized sources of these anions, possibly related to natural or anthropogenic activities occurring near the river. Additionally, an analysis of major cation distribution in the Oyigbo area indicates consistent concentration levels throughout the region, with minimal variability observed. This uniformity suggests a relatively stable environmental condition regarding cationic presence across the area. Importantly, all measured concentrations conform to the standards set by the World Health Organization (WHO, 2017), emphasizing the environmentally acceptable levels of cations present in the area. This adherence to established standards underscores the overall health and safety of the environmental conditions regarding cationic presence, providing reassurance regarding potential impacts on human health and ecosystem integrity.

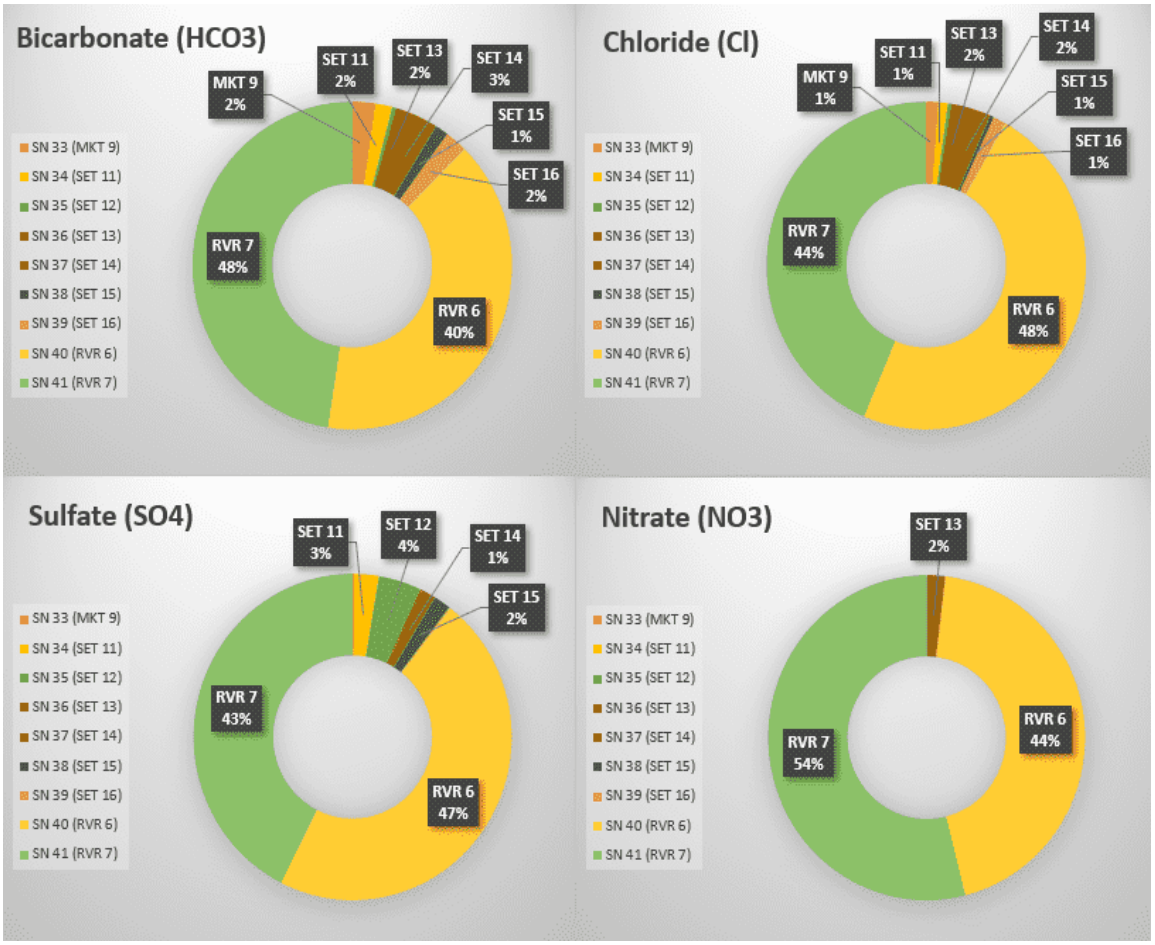

Fig 4e. Percentage Spreading of Anions in Umu Agbai-Obete Axis

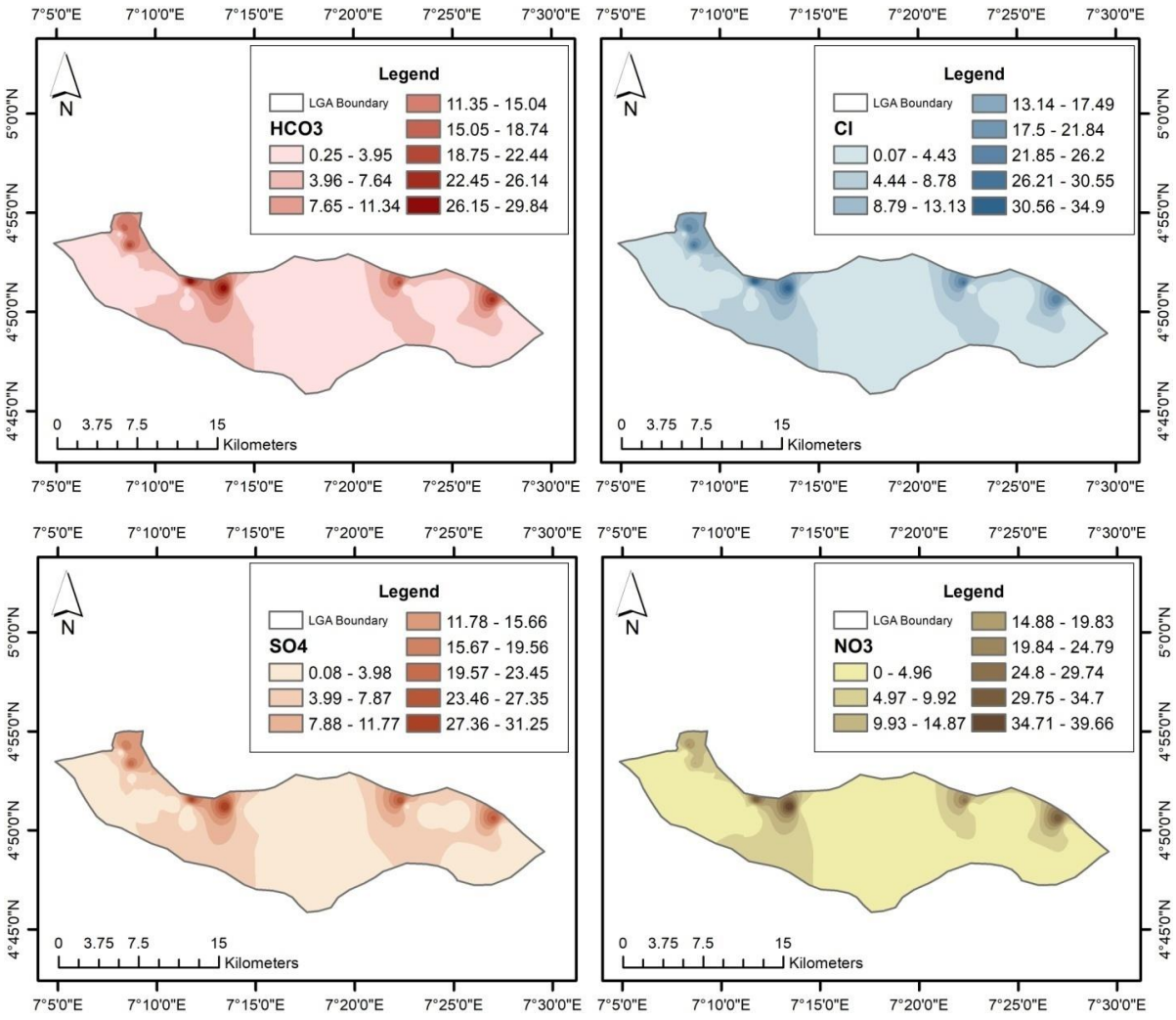

Fig 5. Geospatial Dispersion Maps of Anions across the Study Area

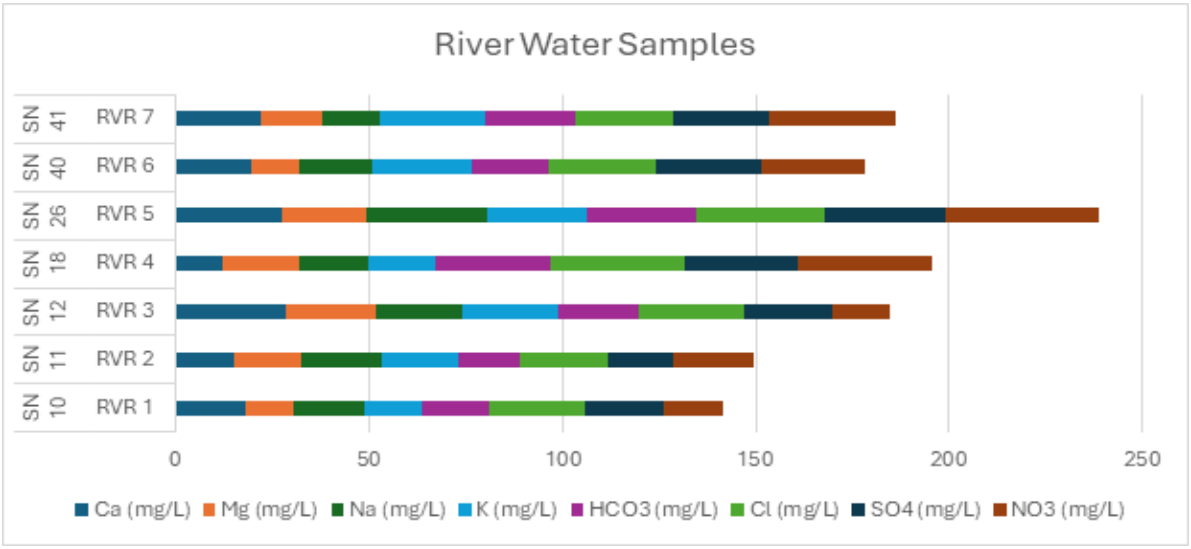

Fig 6a. Stacked Distribution of Cations and Anions in River Water across the Study Area

In general, the analysis of river water samples reveals a diverse range of cation concentrations and distribution for calcium (Ca), sodium (Na), potassium (K), and magnesium (Mg), each falling within distinct ranges. Specifically, Ca concentrations ranged from 12.16 mg/L to 28.71 mg/L, Na concentrations from 14.93 mg/L to 31.05 mg/L, K concentrations from 14.63 mg/L to 26.99 mg/L, and Mg concentrations from 12.37 mg/L to 23.21 mg/L (Figure 6a). Conversely, rainwater samples displayed different concentration ranges, with Ca concentrations spanning from 0.02 mg/L to 4.02 mg/L, Na concentrations from 0.08 mg/L to 1.89 mg/L, K concentrations from 0.09 mg/L to 1.75 mg/L, and Mg concentrations from 0.01 mg/L to 1.078 mg/L (Figure 6b). Importantly, all measured cation concentration values fell within the standards set by the World Health Organization (WHO), indicating compliance with acceptable limits. Moving on to anions in river water, the concentrations of HCO3 ranged from 15.71 mg/L to 29.85 mg/L, Cl from 22.63 mg/L to 34.92 mg/L, SO4 from 19.86 mg/L to 31.29 mg/L, and NO3 from 15.12 mg/L to 39.72 mg/L. Similarly, rainwater concentration values for HCO3 ranged from 0.45 mg/L to 2.13 mg/L, Cl from 0.07 mg/L to 2.11 mg/L, SO4 from 0.08 mg/L to 3.91 mg/L, and NO3 from 0.001 mg/L to 1.22 mg/L.

In the study area, particularly in regions near petroleum production facilities, there is a notable elevation in sulfate (SO4) concentrations in water, especially, in the rainwater. This increase could be primarily attributed to emissions from gas flaring, which releases sulfur dioxide (SO2) that reacts with atmospheric oxygen and water vapor to form sulfuric acid (H2SO4), leading to sulfate deposition (Okorhi-Damisa, et al., 2020). Industrial discharges from petroleum operations and disturbances to surface water and soils also contribute to sulfate release into the environment. Heightened sulfate levels pose risks to aquatic ecosystems by potentially forming toxic hydrogen sulfide (H2S) and disrupting pH balance, affecting aquatic life and biodiversity. Human health concerns could arise from consuming water with elevated sulfate concentrations, leading to gastrointestinal issues (Ahmed et al., 2024b). However, despite these concerns, all measured sulfate concentrations including all other major ions in both river and rainwater samples fell within acceptable limits according to WHO standards, indicating satisfactory water quality with respect to ionic presence.

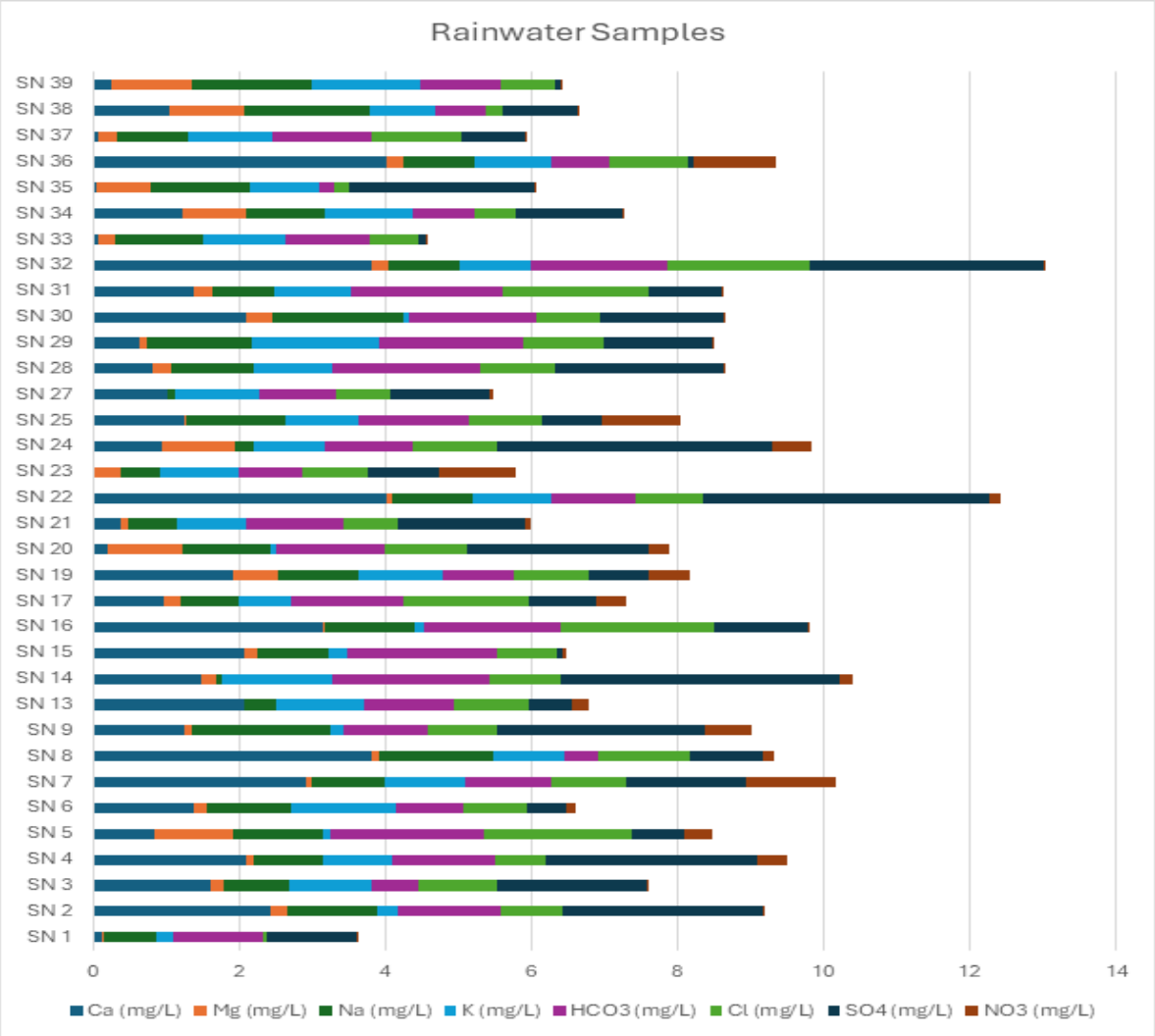

Fig 6b. Stacked Distribution of Cations and Anions in Rainwater across the Study Area

3.2 Hydrochemical Characterization

3.2.1 Piper Diagram

The Piper Trilinear plot (Piper, 1944) is a highly effective tool for groundwater quality assessments, providing detailed insights into water geochemistry that surpass those offered by other plotting techniques (Sakram et al., 2013). The Piper trilinear diagram for river water and rainwater samples (Figure 7a and 7b) illustrates a Ca2+-Mg2+-Cl--SO42- facies, signifying the dominance of alkaline earth metals over alkali metals and the presence of strong acidic anions in greater abundance than weak acidic anions. According to Langguth's (1996) classification for Piper diagrams, this water type is categorized as alkaline earth water with increased alkalis and a predominance of sulfate and chloride ions. The cation plot suggests a calcium-rich water type, while the anion plot indicates a higher concentration of Cl- and SO42- compared to HCO3-.

The positioning of these water samples on the Piper diagram indicates a mixed water type. For river water samples, Ca and Mg emerge as the dominant cationic species, while Cl is the predominant anionic species (Figure 7a).

This suggests that the river water chemistry is influenced by the dissolution of minerals from surrounding rocks and soils, as well as potential contributions from anthropogenic sources such as agricultural runoff and industrial discharges. The Piper plot further illustrates that the river water samples fall into the calcium chloride water type, reflecting geochemical processes like mineral weathering and potential contamination from chloride-bearing sources.

Similarly, rainwater samples exhibit a dominance of Ca and Mg in the cationic area (Figure 7b), with Cl being the dominant anionic species. This composition is indicative of atmospheric deposition processes, where airborne particles rich in calcium and chloride from both natural sources (e.g., sea spray, soil dust) and anthropogenic activities (e.g., industrial emissions, vehicular exhaust) are scavenged by precipitation. The rainwater's chemical signature places it in the mixed water type category, with a tendency towards calcium chloride water type, akin to the river water samples. The geochemical zone 6, as identified on the Piper diagram, indicates the prevalence of calcium chloride water type and mixed water type in the study area.

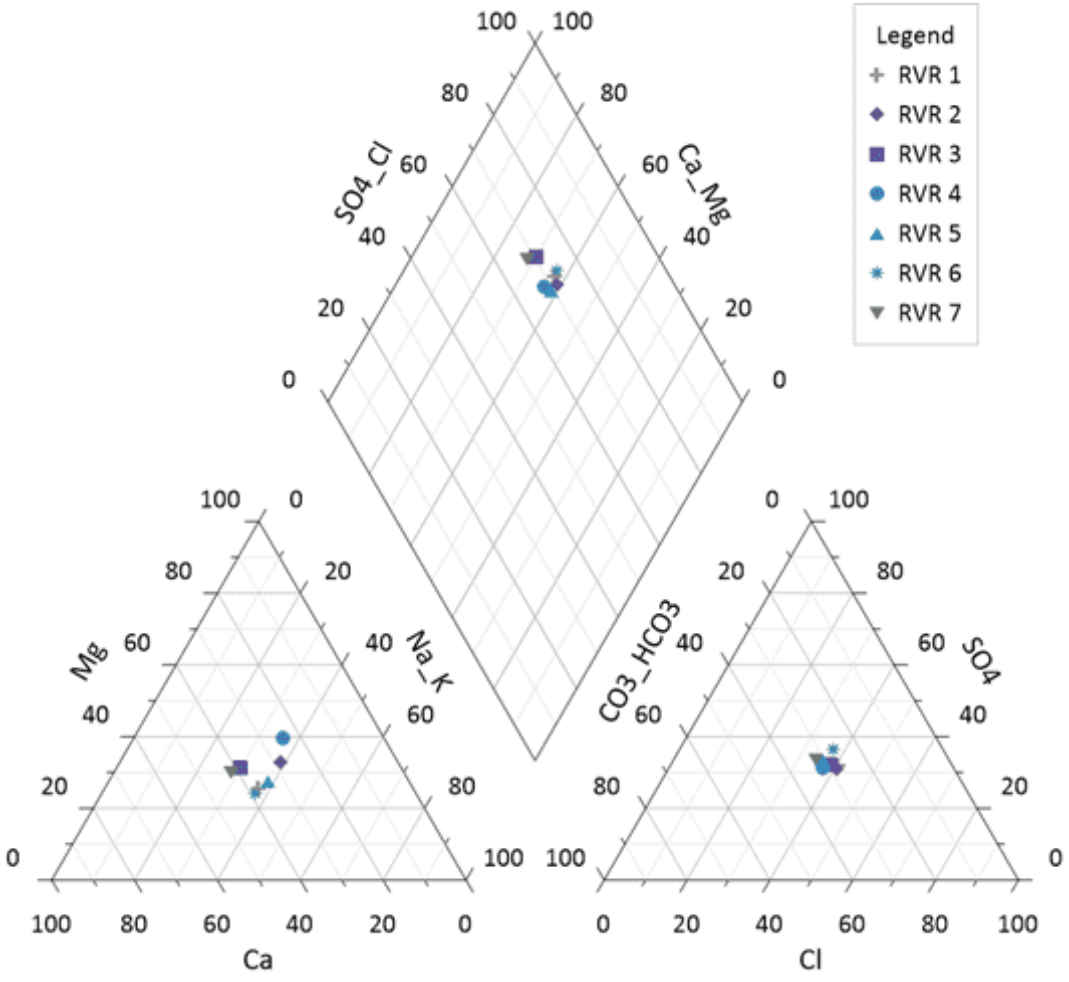

Fig 7a. Piper Diagram for River Water Samples

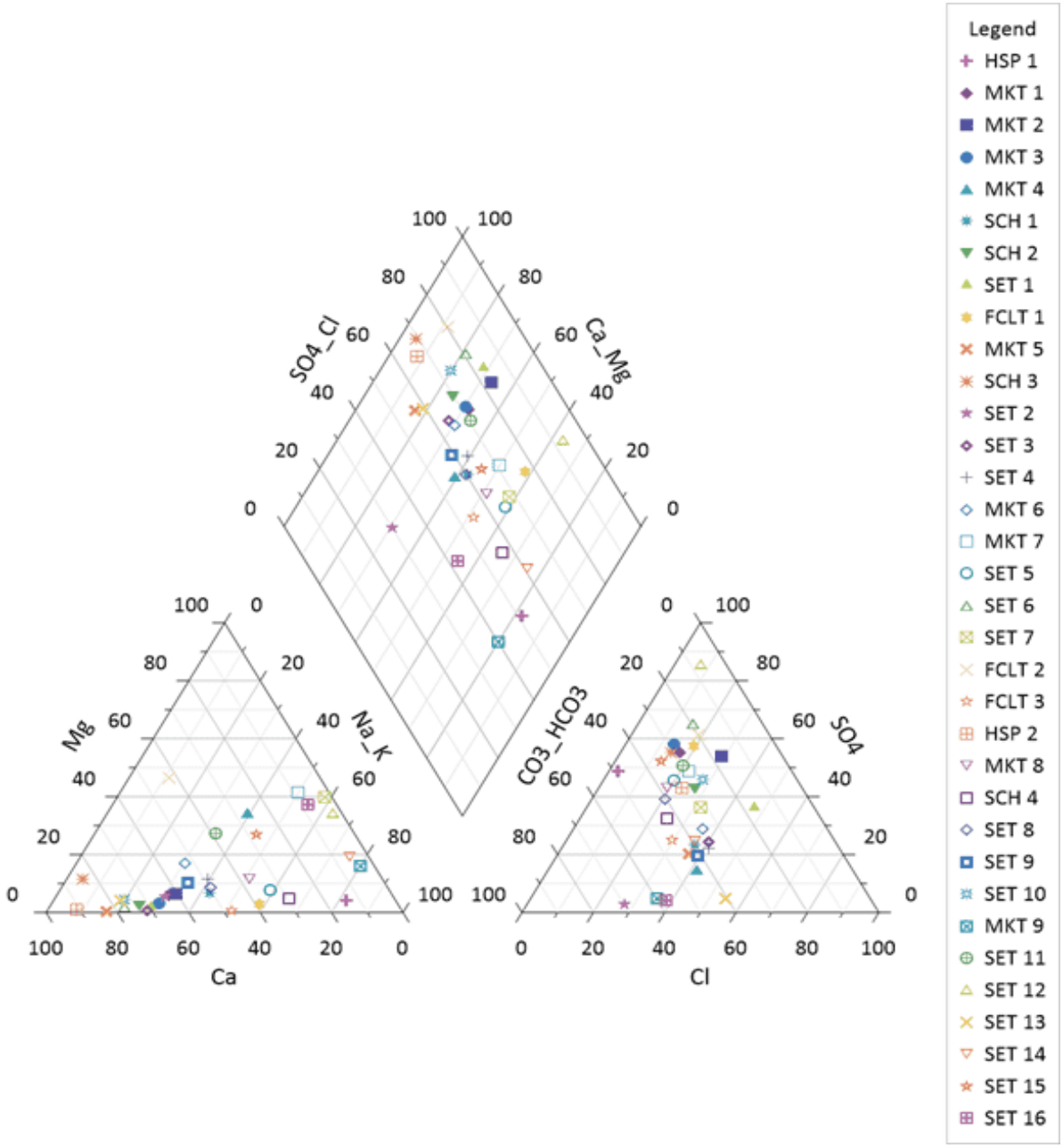

Fig 7b. Piper Diagram for Rainwater Samples

The presence of chlorides in both river water and rainwater samples could stem from various sources such as rocks, evaporites, seawater intrusion, connate and juvenile water, or contamination from industrial or domestic sources (Saha et al., 2019; Egbueri, 2019). In coastal regions, seawater intrusion can significantly influence groundwater chemistry, especially in over-extracted aquifers. Inland, the dissolution of evaporite minerals and anthropogenic inputs are common chloride sources.

The findings from this study contrast with those from similar studies conducted in different geographical locations, such as Bangladesh (Saha et al., 2019) and Nigeria (Egbueri, 2019; Akakuru et al., 2021). These differences underscore the unique geochemical characteristics and influences at play in the local water sources of the study area. For instance, while the study area shows a significant presence of calcium chloride water type, other regions might exhibit different dominant ions and water types due to varying geological formations, climatic conditions, and anthropogenic impacts.

Overall, the use of the Piper Trilinear plot in this study has provided a comprehensive understanding of the geochemical composition of water samples, revealing significant differences between river water and rainwater. The detailed analysis emphasizes the importance of considering multiple sources and processes in water quality assessments. These insights are crucial for developing informed water management and conservation strategies, addressing potential contamination sources, and ensuring the sustainable use of water resources in the study area.

3.2.2 Durov Diagram

In this study, the Durov diagram, alongside the Piper plot, was employed to analyze and interpret the geochemical characteristics of water samples, as depicted in Figures 8a and 8b. The Durov diagram involves plotting cations and anions as percentages on separate triangular diagrams. By extending lines from these plotted points, their intersection indicates specific water types (Durov, 1948). Further analysis involves drawing lines from these intersection points to adjacent rectangles, which helps determine the total ion concentration (measured in mg/L or g/L) and facilitates the assessment of the chemical composition of the water samples.

The use of the Durov diagram for geochemical modeling provides intricate insights into the water composition in the study area (Sakram et al., 2013). Specifically, the analysis of river water samples reveals patterns indicative of simple dissolution or mixing processes, which govern their chemical makeup. These processes are represented by linear trends on the diagram, suggesting that the river water is influenced by the dissolution of minerals or the mixing of different water sources.

In contrast, the analysis of rainwater samples plotted on the Durov diagram highlights a significant presence of calcium and sulphate ions. This distinct calcium-rich and sulphate-rich water type is indicative of specific geochemical processes and sources. The rainwater's chemical composition suggests it may be influenced by atmospheric deposition of calcium and sulphate, possibly from natural sources like soil dust or anthropogenic activities such as industrial emissions.

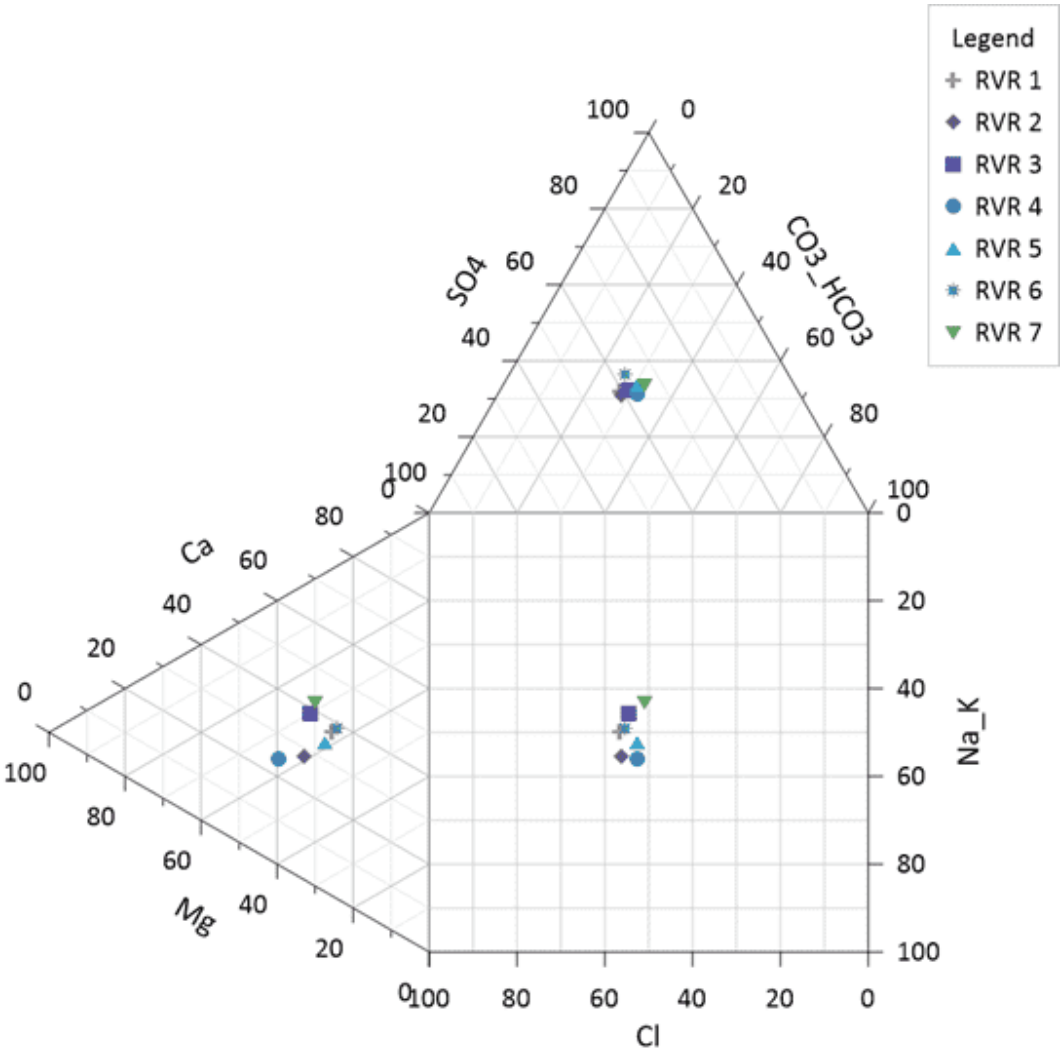

Fig 8a. Durov Diagram for River Water Samples

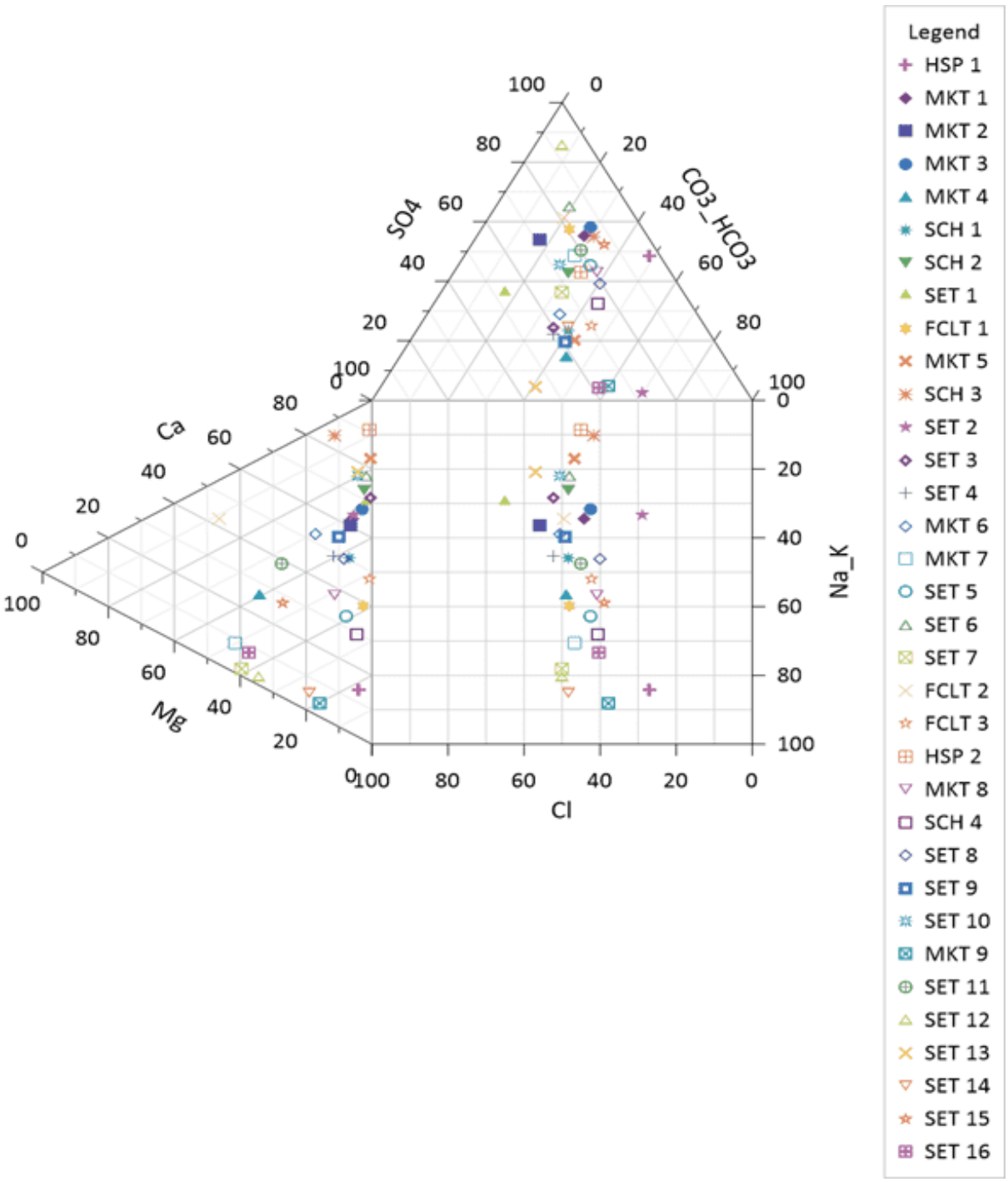

Fig 8b. Durov Diagram for Rainwater Samples

This discrepancy between the geochemical characteristics of surface water and rainwater underscores the diverse influences shaping their composition. The river water's chemical makeup appears to be controlled by local geological formations and the dissolution of minerals, while the rainwater's composition reflects atmospheric contributions and potentially distant sources.

These findings prompt a more detailed investigation into the factors contributing to the observed variations in water composition. Such factors may include natural processes, such as weathering of rocks and soil erosion, as well as anthropogenic activities like agriculture, industrial emissions, and urban runoff. Understanding the interplay between these factors is crucial for developing effective water management strategies and mitigating potential impacts on water quality.

The use of the Durov diagram and Piper plot in this study has provided a comprehensive understanding of the geochemical dynamics of water samples in the study area. By identifying the distinct chemical characteristics of river water and rainwater, this analysis highlights the need for further research into the sources and processes influencing water quality. Such insights are essential for informed decision-making and the implementation of sustainable water management practices.

3.2.3 Schoeller Semi Logarithmic diagram

The Schoeller diagram according to (Schoeller, 1967) depicted in Figure 9a and 9b offers valuable insights into the hydrogeochemical trends observed in the study area. For surface water samples, the trend indicates a sequence of constituents in descending order of abundance, with magnesium (Mg+) occupying the highest proportion followed by chloride (Cl+), calcium (Ca+), sodium and potassium (Na++K+), sulphate (SO42-), nitrate (NO3-), and bicarbonate (HCO3-), which has the lowest concentration. In contrast, the hydrogeochemical trend for rainwater samples reveals a different sequence, with calcium (Ca+) being the most abundant, succeeded by sulphate (SO42-), magnesium (Mg+), sodium and potassium (Na++K+), chloride (Cl+), bicarbonate (HCO3-), and nitrate (NO3-), which appears to have the lowest concentration. For surface water samples the trend simply follows the pattern Mg+ > Cl+ > Ca+ > Na++K+ >SO42-> NO3-> HCO3-, in the order of the highest to the lowest constituent.

While, for the rainwater samples, the trend was Ca+ > SO42-> Mg+ > Na++K+ >Cl+ > HCO3- > NO3-, in the order of the highest to the lowest constituents. These trends highlight the distinct chemical compositions of surface water and rainwater in the study area, providing valuable information about the dominant ions present and their relative concentrations. The semi-logarithmic plot presented a correlation with the water type observed in the plots (Falah and Haghizadeh, 2017). In this plot, upward points indicate the prevalence of dominant ions in the samples, while downward points suggest a lower presence of ions, indicating fewer ions available. Unlike other graphs that commonly utilize either arithmetic or logarithmic scales to represent water quality data, this semi-logarithmic plot offers distinct advantages, especially when comparing low-concentration waters or those with minimal differences in concentration (Piri and Kisi, 2017). Its unique scale allows for clearer visualization and analysis of subtle variations in ion concentrations, making it particularly useful in such contexts.

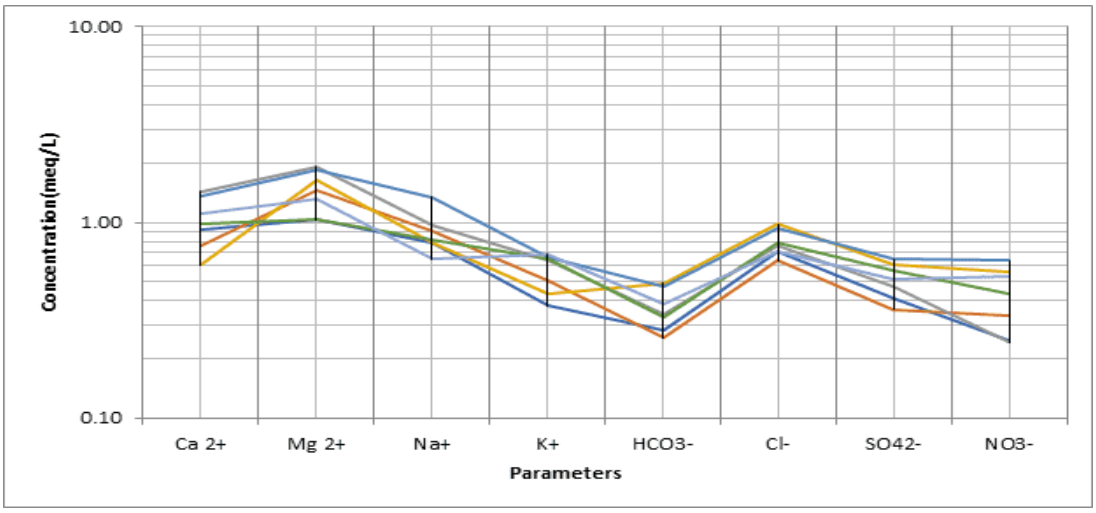

Fig 9a. Schoeller Plot of the Major Ions Distribution Pattern with High-Low Lines in the River Water

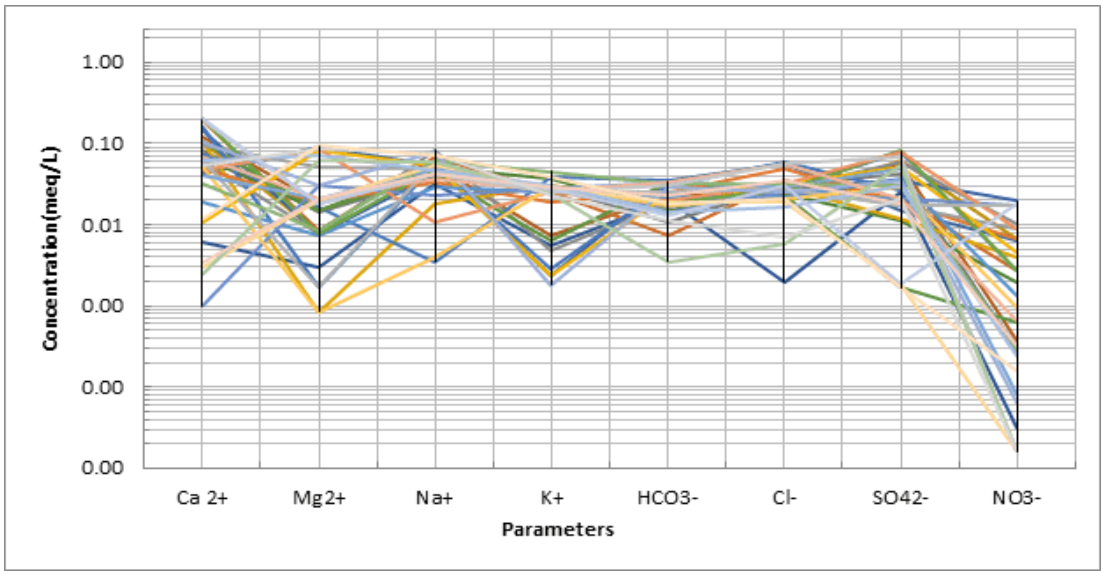

Fig 9b. Schoeller Plot of the Major Ions Distribution Pattern with High-Low Lines in the Rainwater

4. Conclusion

The study employed geospatial analysis and various geochemical models including the Piper Trilinear plot, Durov diagram, and Schoeller diagram, to characterize the ionic composition of surface water and rainwater around selected petroleum producing areas in Oyigbo, Local Government Area (L.G.A.), South-Southern Nigeria. The spatial distribution of cations and anions, including Ca, Mg, Na, K, HCO3, Cl, SO4, and NO3, reveals a relatively uniform pattern across the study area, with higher concentrations observed along the river channel, particularly in the upper region at the Northwestern, Northern, and Northeastern sections from the Obigbo, through Komkom-Obiama to Okoloma Axis of Oyigbo L.G.A. This suggests potential localized sources, possibly related to natural or anthropogenic activities near the river. Rainwater samples exhibit lower concentrations compared to the river system, with discernible variations in concentration, particularly higher in areas adjacent to petroleum activities or production facilities. The Piper Trilinear plot revealed that Ca + Mg dominated as cations, while Cl emerged as the dominant anion in both river water and rainwater samples. Moreover, the Durov diagram depicted a simple dissolution or mixing line in river water, contrasting with rainwater samples which exhibited notable presence of calcium and sulphate. Additionally, the Schoeller diagram showcased distinct hydrogeochemical trends, with surface water showing Mg+ > Cl+ > Ca+ > Na++K+ >SO42-> NO3-> HCO3-, and rainwater showing Ca+ > SO42-> Mg+ > Na++K+ >Cl+ > HCO3- > NO3-. These trends suggested a calcium chloride water type, with rainwater displaying heightened calcium and sulphate concentrations. Geospatial analysis highlighted consistent ion concentration levels throughout the Oyigbo area, implying environmental stability. Despite concerns about increased sulfate near petroleum facilities, all measured ion concentrations in both river and rainwater samples adhered to WHO standards, indicating satisfactory water quality in terms of ionic presence.

References

Abugu, H. O., Egwuonwu, P. F., Ihedioha, J. N., & Ekere, N. R. (2021). Hydrochemical evaluation of River Ajali water for irrigational application in agricultural farmland. Applied Water Science, 11, 71. https://doi.org/10.1007/s13201-021-01395-4.

Adejuwon, J. O. (2012). Rainfall seasonality in the Niger delta belt, Nigeria. Journal of Geography and Regional Planning, 5(2), 51.

Adeyeye, J. A., Akintan, O. B., & Adedokun, T. (2019). Physicochemical characteristics of harvested rainwater under different rooftops in Ikole Local Government Area, Ekiti State, Nigeria. Journal of Applied Sciences and Environmental Management, 23(11), 2003-2008.

Ahmed, N. O., & Taiwo, O. S. (2023). Spatio-temporal analysis of Ilorin Airport on the land-use of Ilorin metropolis, Southwestern Nigeria. Journal of Applied Geospatial Information (JAGI), 7(2), 948-955. https://doi.org/10.30871/jagi.v7i2.5693.

Ahmed, N. O., & Udom, G. J. (2024a). Chemophysical and Metallic Characterization of Surface Water and Precipitation for Environmental Quality Assessment in Oyigbo L.G.A., Rivers State, Nigeria. Journal of Global Ecology and Environment, 20(1), 28–57. https://doi.org/10.56557/jogee/2024/v20i18562.

Ahmed, N. O., Obafemi, A. A., & Udom, G. J. (2024b). Geospatial variability and distribution of total petroleum hydrocarbons (TPH) in soot-contaminated rain and rivers at Oyigbo, Niger Delta, Nigeria. Journal of Geography, Environment and Earth Science International, 28(3), 1–30. https://doi.org/10.9734/jgeesi/2024/v28i3753.

Akakuru, O. C., Akudinobi, B., Opara, A. I., Onyekuru, S. O., & Akakuru, O. U. (2021). Hydrogeochemical facies and pollution status of groundwater resources of Owerri and environs, Southeastern Nigeria. Environmental Monitoring and Assessment, 193, 623.

Akter, T., Jhohura, F. T., Akter, F., Chowdhury, T. R., Mistry, S. K., Dey, D., Barua, M. K., Islam, M. A., & Rahman, M. (2016). Water quality index for measuring drinking water quality in rural Bangladesh: A cross-sectional study. Journal of Health, Population, and Nutrition, 35(4). https://doi.org/10.1186/s41043-016-0041-5.

Anslem, O. A. (2013). Negative effects of gas flaring: The Nigerian experience. Journal of Environment Pollution and Human Health, 1(1), 6–8.

Appelo, C. A. J., & Postma, D. (1993). Geochemistry, groundwater and pollution (2nd ed.). Balkema.

Bhardwaj, K., Boora, N., & HAU, H. (2023). Water Quality Parameter. In S. Sharma (Ed.), Shweta Sharma (pp. 78).

Chaniago, M. D., & Taki, H. M. (2022). Geographic Information System (GIS) as an information media in the field of environmental health: Literature review. Journal of Applied Geospatial Information, 6(2), 641-646. https://doi.org/10.30871/jagi.v6i2.4319.

Chen, D., & Guo, Z. (2022). The Source, Transport, and Removal of Chemical Elements in Rainwater in China. Sustainability, 14(19), 12439.

Cidu, R., Frau, F., & Tore, P. (2011). Drinking water quality: Comparing inorganic components in bottled water and Italian tap water. Journal of Food Composition and Analysis, 24(2), 184–193

Durov, S. A. (1948). Classification of natural waters and graphical representation of their composition. Doklady Akademii Nauk SSSR, 59(1), 87-90.

Edet, A. (2018). Seasonal and spatio-temporal patterns, evolution and quality of groundwater in Cross River State, Nigeria: Implications for groundwater management. Sustainable Water Resources Management, 5(2), 667–687. https://doi.org/10.1007/s40899-018-0236-6.

Egbueri, J. C., Mgbenu, C. N., & Chukwu, C. N. (2019). Investigating the hydrogeochemical processes and quality of water resources in Ojoto and environs using integrated classical methods. Model. Earth Syst. Environ., 5, 1443–1461.https://doi.org/10.1007/s40808-019-00613-y.

Falah, F., & Haghizadeh, A. (2017). Hydrochemical evaluation of river water quality—a case study: Horroud River. Applied Water Science, 7, 4725–4733. https://doi.org/10.1007/s13201-017-0635-0.

Fawole, O. G., Cai, X. M., & MacKenzie, A. R. (2016). Gas flaring and resultant air pollution: A review focusing on black carbon. Environmental Pollution, 216, 182-197.

Idris, M. K., Hasri, M., & Setyaningsih, W. A. (2021). Mapping and monitoring of environmental conditions in Cilacap waters. *Journal of Applied Geospatial Information,* *5*(1), 437-444. https://doi.org/10.30871/jagi.v5i1.2838

Khatri, N., & Tyagi, S. (2015). Influences of natural and anthropogenic factors on surface and groundwater quality in rural and urban areas. Frontiers in Life Science, 8(1), 23-39.

Langguth, H. R. (1996). Groundwater characteristics in Bereich des Velberter Sattles (p. 127). North Rhine-Westphalia: Ministry of Agricultural and Land Management Research Duesseldorf.

Li, P., Zhang, Y., Yang, N., Jing, L., & Yu, P. (2016). Major ion chemistry and quality assessment of groundwater in and around a mountainous tourist town of China. Expo Health, 8, 239–252. https://doi.org/10.1007/s12403-016-0198-6.

Li, R. Z., Pan, C. R., Xu, J. J., Ding, G. Z., & Zou, Y. (2012). Application of potential ecological risk assessment model based on Monte Carlo simulation. Res. Environ. Sci., 25, 1336–1343.

Liu, C., Zhang, J., Li, F., Yang, J., Qiu, Z., Cai, Y., Zhu, L., Xiao, M., & Wu, Z. (2018). Trace elements spatial distribution characteristics, risk assessment and potential source identification in surface water from Honghu Lake, China. Journal of Central South University, 25(7), 1598–1611. https://doi.org/10.1007/s11771-018-3852-2.

Mir, A., Piri, J., & Kisi, O. (2017). Spatial monitoring and zoning water quality of Sistan River in the wet and dry years using GIS and geostatistics. Computers and Electronics in Agriculture, 135, 38-50. https://doi.org/10.1016/j.compag.2017.01.022.

NBS (2006). National Bureau of Statistics – Nigeria: Social Statistics Report.

Ochelebe, I., & Kudamnya, E. A. (2022). Hydrochemistry and an appraisal of surface water and groundwater quality for domestic and irrigation use in parts of Southern Benue Trough, Nigeria. Sustainable Water Resources Management, 8, 174. https://doi.org/10.1007/s40899-022-00762-6.

Ochelebe, I., Kudamnya, E. A., & Nkebem, G. E. (2020). An assessment of heavy metals concentration in water around quarries and barite mine sites in part of central Cross River State, southeastern Nigeria. Global Journal of Geology and Earth Science, 18(2020), 89–95.

Ofgeha, G. Y., & Abshire, M. W. (2021). Spatio-temporal variability and trends in rainfall and temperature in Anger watershed, Southwestern Ethiopia. *Journal of Applied Geospatial Information, 5*(1), 462-472. https://doi.org/10.30871/jagi.v5i1.2825.

Okorhi-Damisa, F. B., Ogunkeyede, A. O., Akpejeluh, P., & Okechukwu, L. (2020). Analysis of soot in rainwaters around Warri metropolis. International Journal of Scientific Development and Research, 5(5), 319–325.

Olowoyo, D. N. (2011). Physicochemical characteristics of rainwater quality of Warri axis of Delta state in western Niger Delta region of Nigeria. Journal of Environmental Chemistry and Ecotoxicology, 3(12), 320-322.

Onwuka, C., Eboatu, A. N., Ajiwe, V. I. E., & Morah, E. J. (2021). Pollution studies on soils from crude oil producing areas of rivers state, Niger delta region, Nigeria. Open Access Library Journal, 8(9), 1-17.

Orji, D., Ndu, A., Ihesinachi, K., & Adaunwo, E. O. (2019). The total petroleum hydrocarbon contents of the ambient air within Port Harcourt and environs. Chemistry Research Journal, 4(3), 117–123.

Piper, A. M. (1944). A graphic procedure in the geochemical interpretation of water-analyses. Eos, Transactions American Geophysical Union, 25, 914-928. http://dx.doi.org/10.1029/TR025i006p00914.

Roșca, O. R., Dippong, T., Marian, M., Mihali, C., Mihalescu, L., Hoaghia, M., & Jelea, M. (2020). Impact of anthropogenic activities on water quality parameters of glacial lakes from Rodnei mountains, Romania. Environmental Research, 182, 109136. https://doi.org/10.1016/j.envres.2020.109136.

Saha, S., et al. (2019). FunPred 3.0: Improved protein function prediction using protein interaction network. PeerJ, 7, e6830.

Sakram, G., Sundaraiah, R., Vishnu Bhoopathi, & Praveen Raj Saxena. (2013). The impact of agricultural activity on the chemical quality of groundwater, Karanjavagu watershed, Medak district, Andhra Pradesh. International Journal of Advanced Scientific and Technical Research, 6(3), Nov.-Dec. 2013.

Samuel, P., Elechi, O., & Julius, N. E. (2022). Total Hydrocarbon Contents: Spatial Variations in Aquatic Environment of Oyigbo Communities, Rivers State. International Journal of Environmental Protection and Policy, 10(1), 1-5.

Schoeller, H. (1967). Qualitative evaluation of groundwater resources. In H. Schoeller (Ed.), Methods and techniques of groundwater investigation and development (Water Resource Series No. 33, pp. 44-52). UNESCO.

Shankar, K., Elangovan, G., Balamurugan, P., & Saravanan, R. (2022). Spatial distribution of groundwater quality assessment using Water Quality Index and GIS techniques in Thanjavur Taluk, Thanjavur District, Tamil Nadu, India. International Journal of Civil, Environmental and Agricultural Engineering, 4(2), 32–58.

Singh, R. L., & Singh, P. K. (2017). Global environmental problems. In Principles and applications of environmental biotechnology for a sustainable future (pp. 13-41).

Tiwari, A. K., Ghione, R., Maio, M. G., & Lavy, M. (2017). Evaluation of hydrogeochemical processes and groundwater quality for suitability for drinking and irrigation purposes: A case study in Aosta Valley region, Italy. Arabian Journal of Geosciences, 10(12), 264.

World Health Organization. (2017). Guidelines for drinking-water quality (4th ed. incorporating the first addendum). Geneva, Switzerland. [Accessed: February 25, 2024] Retrieved from http://apps.who.int/iris/bitstream/10665/254637/1/9789241549950-eng.pdf?ua=1.